

A Final Report on

Thin-film Solar Cells for Space Applications

Grant #NAG3-2303

from NASA's Partnership Awards for
Innovative and Unique Education and Research Announcement
NRA 99-OEOP-4

Period covering July 1999 to September 2002

Submitted January 31, 2003

Principal Investigator
Gregory B. Lush, Ph.D.

Department of Electrical and Computer Engineering
University of Texas at El Paso
500 W. University Ave.
El Paso, Texas 79968

Overview and Relevance to NASA

The proposed work supports MURED goals by fostering research and development activities at Fisk and UTEP which contribute substantially to NASA's mission, preparing faculty and students at Fisk and UTEP to successfully participate in the conventional, competitive research and education process, and increasing the number of students to successfully complete degrees in NASA related fields. The project also addresses directly a core need of NASA for space power and is consistent with the Core Responsibilities of the John Glenn Space Center.

Current orbital missions are limited by radiation from high energy particles trapped in the Van Allen Belt because that solar radiation degrades cell performance by damaging the crystalline lattice. Some potential orbits have been inaccessible because the radiation is too severe. Thin-film solar cells, if they can be adapted for use in the unfriendly space environment, could open new orbits to satellites by providing a radiation hard source of power.

The manned mission to Mars requires photovoltaic devices for both the trip there and as a power supply on the surface. Solar arrays using thin films offer a low power/weight ratio solution that provides reliable photovoltaic power.

Goals of the Project

This project proposes to conduct basic material and device studies of thin-film solar cells for space applications. Thin films offer a light-weight and potentially high-efficiency alternative to devices made with crystalline semiconductors. It is expected that thin-film cells will also be more radiation hard, providing a longer lasting power supply. Because of their structure and manner of interconnection, thin-film devices could also be more resilient against particle bombardment.

UTEP's has focused significant resources on developing its capabilities for the fabrication of CdTe solar cells, performing characterization on its own cells and on samples obtained from other sources, and on developing a computer based analysis and simulation tool for thin-film devices.

Fisk's goals were to modify their laser ablation chamber for pulsed laser deposition (PLD), establish the energy density threshold for PLD, evaluate the film properties, including stoichiometry, optical properties (energy gap, static and time gated PL), surface morphology, and electrical properties. Finally, Fisk intended to lay the foundation for making pn or other types of rectifying junctions.

Comparison of Performance with Goals

Fisk University has used its pulsed laser ablation techniques to fabricating high quality, stoichiometric, polycrystalline films of CuInS_2 (CIS) by irradiating a target composed of Cu_2S and In_2S_3 . Experiments were performed to establish the laser parameters of wavelength, energy, and pulse duration for fabricating the CIS films. Extensive characterization of these films are documented in the published papers.

The current studies demonstrate that high quality CIS films can be fabricated by pulsed laser deposition. The characterization of these films indicates that they possess a stoichiometry and structure required for development into solar energy cell materials. Further progress is being made to form rectifying junctions.

UTEP has accomplished all goals related to the device analysis and simulation code development and continued progress with its fabrication goals. UTEP has completed and tested

the infrastructure of a distributed object computational system to be used once the analysis and simulation code is written. The distributed object computational system improves computational performance over the performance of the fastest computer in our computer network by several times. UTEP has also developed further its unique characterization capabilities, making a significant contribution to the area's understanding of junction behavior. The appendix contains three publications of relevance to the project.

Students

At UTEP, four graduate students and fifteen undergraduates have been supported on this project. The students are: Hector Garces (G), Venu Tammabatula (G), Pratima Goud (G), Yuhua Liu (G), Phuntsho Gyaltshen (U), Rosalinda Carrasco (U), Tanya Bell (U), John Delk (U), Dennis Davis (U), Oscar Quintero (U), Hector Escobar (U), James Benoit (U), Angelica Zepeda (U), Casey Cook (U), Jose Fresquez (U), Christina Robinson (U), Ivan Hernandez (U), Franz Kuhlmann (U), and David Dils (U). At Fisk, undergraduates Vanessa Saunders, Thurston Livingston, Charlene Lake, and Carlton Maxwell were supported as were Masters students Dennis Denmark, Elana Bryant, and Mekkonen Bayesseie.

Of the 26 students supported, 21 were minorities, women, or both.

The following publications and conference presentations are results of the work supported under this grant thus far, not just this fiscal year.

Publications and Conference Presentations

Aloysius F. Hepp, Mark A. Smith, John H. Scofield, John E. Dickman, Gregory B. Lush, Donald L. Morel, Christos Ferekides, and Neelkanth G. Dhere, "Multi-Junction Thin-Film Solar Cells on Flexible Substrates for Space Power," Intersociety Energy Conversion Engineering Conference, Washington, D.C., September 2002.

D.L. Linam, V.P. Singh, J.C. McClure, G.B. Lush, X. Mathew, P.J. Sebastian, "Light and voltage dependence of the junction transport properties of CdTe/CdS photovoltaics," *Solar Energy Materials and Solar Cells*, **70**, pp. 335-344, 2001.

D. L. Linam, V. P. Singh, J. C. McClure, G. Lush, X. Mathew, J. Sebastian, "Light and Voltage Dependence of the Junction Transport Properties of CdTe/CdS Photovoltaics," International Materials Research Congress, Cancun, Mexico, August 27 – 31, 2000.

"Non-Uniformity of Short Circuit Current in Thin-Film CdTe-CdS Solar Cells," D. Dils, G.B. Lush, V.P. Singh, and J. C. McClure, International Materials_ Research Congress, Cancun, Mexico, August 27 – 31, 2000.

"Machine Vision For Solar Cell Characterization," Miguel A. Ordaz and G. B. Lush, Electronic Imaging 2000, San Jose, California, January 2000.

D. Henderson, *et al.*, Science News, **157**, p. 335, (2000)

V.P. Singh, D.L. Linam, D.W. Dils, J.C. McClure, and G.B. Lush, "Electro-optical

characterization and modeling of thin film CdS-CdTe heterojunction solar cells," *Solar Energy Materials and Solar Cells*, **63**, pp. 445-466, 2000.

D. Linam, G.B. Lush, D. Dils, V.P. Singh, and J.C. McClure, "Temperature and Illumination Dependent Junction Transport in CdTe-CdS Solar Cells," XXXth Photovoltaic Specialists Conference, Anchorage, Alaska, September 2000.

D. O. Henderson et al, "Optical and structural characterization of copper indium disulfide films," *J. Materials and Design*, in press.

A. Ueda et al. "Optically measured diffusion constant of oxygen vacancies in MgO," *J. Physics: Condens. Matter* **13**, 5535 (2001).

A comprehensive characterization of copper indium disulfide films, R. Mu et al., Proc. SPIE-Int. Soc. Opt. Eng. (Solar Optical Materials XVI), 116 (1999).

Silicon quantum dots in silica, D.O. Henderson et al., Mat. Res. Soc. Symp. Proc, 551 (Materials in Space Science Technology and Exploration) (1999).

Vacancy clusters on surfaces of Au nanoparticles embedded in MgO, J. Xu, et al. Phys Rev Lett. **83**, 4586 (1999).

Structural and optical properties of gold in MgO: Effects of shape and the interface, E. Bryant, et al. Mat Res. Soc. Symp. (2000) in press.

Optical response of gold nanoparticles in dielectric materials, A. Ueda et al., Mat Res. Soc. Symp. (2000) in press.

Three press releases in Science News, Chemical and Engineering News, and Materials Research Society Bulletin.

If there is some other information that would be of value, please feel free to contact the principal investigator.

Respectfully reported by,



Dr. Gregory B. Lush
Department of Electrical and Computer Engineering
University of Texas at El Paso
500 W. University Ave.
El Paso, Texas 79968
915-747-6632
915-747-7871 (FAX)
lush@ece.utep.edu

APPENDIX

Optical and structural characterization of copper indium disulfide thin films

D.O. Henderson^{a,*}, R. Mu^a, A. Ueda^a, M.H. Wu^a, E.M. Gordon^a, Y.S. Tung^b,
M. Huang^c, J. Keay^c, L.C. Feldman^c, J.A. Hollingsworth^d, W.E. Buhro^d,
J.D. Harris^e, A.F. Hepp^e, R.P. Raffaele^e

^aChemical Physics Laboratory, Department of Physics, Fisk University, Nashville, TN 37208, USA

^bCharles Evans and Associates, 301 Chesapeake Drive, Redwood City, CA 94063, USA

^cDepartment of Physics and Astronomy, Vanderbilt University, Nashville, TN 37208, USA

^dDepartment of Chemistry, Washington University, St. Louis, MO 63130, USA

^eNASA Glenn Research Center, Cleveland, OH 44135, USA

Abstract

Thin films of copper indium disulfide (CuInS_2) were synthesized by spray chemical vapor deposition. Rutherford backscattering measurements were used to determine the composition and thickness of the films. The elemental ratios were found to be within 2% of stoichiometrically correct CuInS_2 . The thickness of the films was found to be approximately $1.0 \mu\text{m}$. An optical band-gap of approximately 1.44 eV for this material was determined by optical transmission spectroscopy. Reflectance spectroscopy identified phonon bands centered at 225, 291 and 317 cm^{-1} . © 2001 Elsevier Science Ltd. All rights reserved.

Keywords: Semi-conductors; Vapour deposition; Optical

1. Introduction

Environmental and energy resource issues have driven scientists, engineers and technologists to develop efficient, renewable and clean energy sources. A primary candidate that may meet these demands is a thin film photovoltaic device. However, several concerns, both practical and fundamental, must be addressed in fabricating and evaluating potential materials for photovoltaic applications. The band-gap energy, absorption coefficient, cost of large-scale production, radiation tolerance and environmental stability are important concerns that must be addressed during the research and development of photovoltaic materials. It is also desirable that the composition of the

photovoltaic material poses a minimal threat to the environment in terms of chemical toxicity.

Copper indium diselenide CuInSe_2 has recently drawn considerable interest in the photovoltaics community because of its large absorption coefficient, suitable band-gap and superior radiation tolerance. A conversion efficiency of 16.9% has been achieved for a CuInSe_2 -based small area device [1]. Four-square-foot modules have been reported with active area efficiencies as large as 9.7% [2]. Photovoltaic devices based on the CuInSe_2 show much less photodegradation as compared to amorphous Si [3–7]. These properties suggest that CuInSe_2 is a material that has great potential for photovoltaic applications. However, reasonable production costs for fabricating CuInSe_2 photovoltaic devices have not been realized. In addition, it should be noted that there are concerns about the toxicity of the selenium compounds used in production and potential problems that they may pose.

* Corresponding author. Tel.: +1-615-329-8622; fax: +1-615-329-8634.

E-mail address: henderson@dubois.fisk.edu (D.O. Henderson).

Another material having the chalcopyrite structure, copper indium disulfide (CuInS_2), has been studied to a lesser extent, but it too possesses properties that indicate it has great potential as a photovoltaic material. The most attractive feature of CuInS_2 is its band-gap of approximately 1.53 eV. This is nearly the optimum band-gap for a single-junction photovoltaic device that is to be used in our solar spectrum, based on theoretical efficiency [8]. The precursor agents that may be used in large-scale fabrication of CuInS_2 are expected to be more cost effective than those used for CuInSe_2 . The issues of toxicity and environmental impact from sulfur-based chalcopyrite photovoltaics are expected to be minimal in comparison to selenium-based devices. The inter-diffusion of sulfur from cadmium sulfide (CdS) (commonly used in heterojunctions) is likely to be less of a problem in causing deviations from stoichiometry near the CdS – CuInS_2 interface, as compared to the CdS – CuInSe_2 interface where Se/S exchange is expected to occur. The precursor materials for fabricating CuInS_2 thin films via spray chemical vapor deposition (CVD) have been developed and show promise for large scale production of solar cells [9]. However, a comprehensive characterization of the fundamental photovoltaic properties of these films and how they depend on growth and process conditions is necessary. Stoichiometry, material morphology, grain structure, optical response and electrical characteristics are just some of the properties that are certain to play a significant role in device performance.

As an initial step in characterizing some of the properties of CuInS_2 films prepared by spray CVD, we report transmission and reflectance spectroscopy, Rutherford backscattering spectrometry (RBS), atomic force microscopy (AFM) and scanning tunneling microscopy (STM) results for CuInS_2 thin films prepared by this method.

2. Experimental

The CuInS_2 films were prepared by spray CVD on quartz substrates. The spray CVD method involves the generation of an aerosol mist of a precursor solution that is generated using a piezoelectric transducer and is transported by an inert carrier gas to a 2-zone, hot-wall furnace for volatilization, decomposition and deposition. Details of the film growth process has been reported elsewhere [9].

A Hitachi UV-Vis-NIR 3501 spectrophotometer was used to optically characterize the CuInS_2 films. In order to eliminate any possible scattering losses due to surface roughness and grain boundaries, an integrating sphere accessory was used to collect transmission spectra. In order to quantify any scattering losses, a conventional transmission measurement without an integrat-

ing sphere was also performed. Reflectance measurements were performed using a 15° angle of incidence and a standard reference mirror.

Fourier transform infrared reflectance measurements were obtained at a 15° angle of incidence. Typically, 400 interferograms were co-added in a single measurement. Sample spectra were normalized using a silver mirror.

A Digital Instrument Nanoscope III tapping mode AFM was used to study the surface roughness of the CuInS_2 films. These measurements were performed with an E scanner capable of scanning a range of $16 \times 16 \mu\text{m}$. The lateral resolution is estimated to be 10–30 nm, depending on the tip used and the tip's history. Several tips were used to minimize tip artifact effects. The z-range accuracy is on the order of 1 nm, depending on the scan size and the surface roughness. The scan rate was 1.5 Hz. No filters were used to obtain images.

Scanning tunneling microscopy (STM) was also used to characterize the surface morphology. A D-scanner head capable of obtaining $15 \times 15 \mu\text{m}$ images was used. A tunneling current set point of 1 nA and a bias voltage of 800 mV were used to acquire the images. Typically, scan rates of 3–4 Hz were used for a scan size of $3 \times 3 \mu\text{m}$. All images were acquired without filtering.

Rutherford backscattering spectrometry (RBS) was performed using singly charged He ions at an energy of 1.8 MeV, under a vacuum of 1×10^{-7} torr. The RBS spectra were collected at a backscattering angle of 160° . The elemental composition of the films was determined by theoretically fitting the RBS spectra.

3. Results and discussion

Fig. 1 shows an RBS channel spectrum of a CuInS_2 film on quartz. As indicated in the figure, the stair-like trace from the high channel energy reflects the elemental composition of the film, In, Cu and S, respectively. The simulation results indicate that the stoichiometry of the CuInS_2 film is S:Cu:In = 2:1:1. The stoichiometric uncertainty for each element is $\pm 2\%$. The amount of error cannot eliminate the possibility that other phases could be present (e.g. Cu_2S , In_2S_3), although it is not expected [10]. Analogous to the $\text{Cu}_x\text{In}_{2-x}\text{Se}_2$ system, a CuIn_5S_8 phase may also be present, however, its concentration would be small based on the measured stoichiometry. In addition, with a $\pm 2\%$ error in stoichiometry, it is impossible to predict if the films are p- or n-type. Film thickness was also determined to be $0.98 \mu\text{m}$ from the RBS spectrum, assuming the density of the film is the same as bulk CuInS_2 (4.74 g/cm^3).

The optical absorption spectrum of CuInS_2 deposited on a quartz surface is shown in Fig. 2. As-

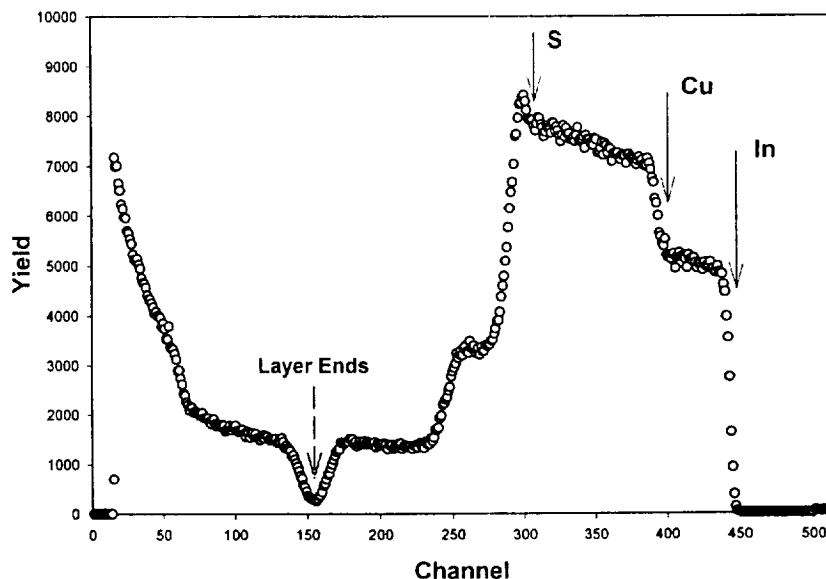


Fig. 1. RBS channel spectrum of a CuInS_2 film on a quartz substrate.

suming CuInS_2 is a direct band gap material, a parabolic band structure approximation can be used to relate the absorbance α to the band-gap energy E_g using:

$$\alpha = C(\hbar\omega - E_g)^{1/2} \quad (1)$$

where $\hbar\omega$ is the incident photon energy, E_g is the optical band-gap and C is a material dependent constant. The inset in Fig. 2 shows the square of the absorbance vs. photon energy. A least-squares fit to the linear portion of this curve yields an x -intercept of 1.44 eV. This value is in relatively good agreement with the previously reported value of 1.5 eV for the optical band-gap of CuInS_2 [11].

The desired thickness of the absorber layer in a thin film solar cell is determined by the absorption coefficient. At 1.5 eV, the optical absorbance from the CuInS_2 film has reached 1.0, indicating that 90% of the

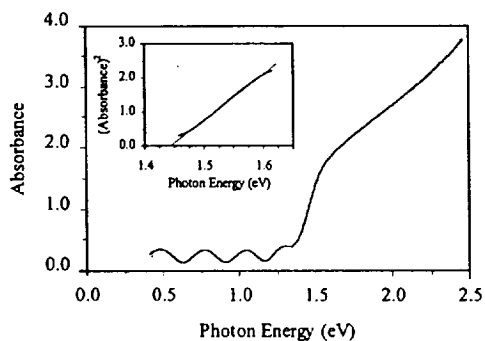


Fig. 2. The optical absorption spectrum of a CuInS_2 film on a quartz substrate. The inset shows a plot of the absorption vs. the photon energy.

photons at that energy are absorbed. Therefore, in terms of film thickness, a 1 μm thick absorption layer of CuInS_2 is sufficient for solar cell applications.

Surface roughness and grain size of polycrystalline thin films have been directly correlated to device efficiency [12]. Surface roughness not only causes light scattering, but it also increases the surface area and interface, which can lead to an increase in the carrier recombination rate. The AFM and STM images, shown in Figs. 3 and 4, provide direct visual information on both grain size and surface roughness. Fig. 3a is a tapping mode AFM image of an as-deposited CuInS_2 film. The surface of the film consists of needle-like grains that have a preferred orientation, with the major axis parallel to the film surface. Grain sizes range from approximately 200–600 nm. The surface roughness is on the order of 100 nm (peak-to-valley difference), as seen in a cross-sectional view (see Fig. 3b). This suggests that mainly UV light (5 eV or higher) would be scattered. Fortunately, the intensity of the solar spectrum at these energies is low and virtually zero on earth's surface. A STM image of the surface was also obtained for this sample (see Fig. 4a). The peak-to-valley differences appear to be slightly less than in the AFM image (see Fig. 4b). The differences in the AFM and STM images are most likely due to tip convolution effects.

The infrared reflectance spectrum of the CuInS_2 film shows three peaks located at 225, 291 and 317 cm^{-1} (see Fig. 5). The infrared spectrum is in good agreement with the literature [11]. However, the values of 323 and 352 cm^{-1} for the longitudinal optical phonon (LO) and transverse optical phonon (TO) frequencies

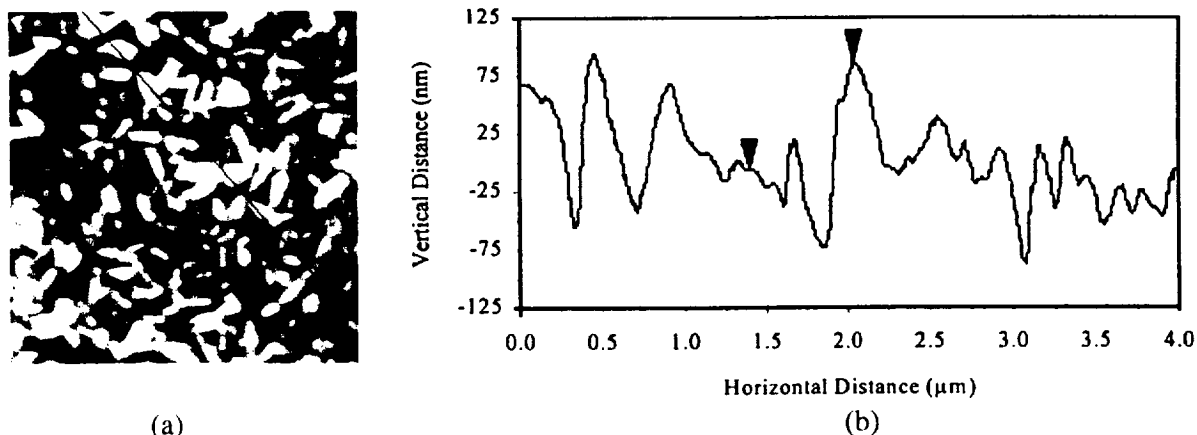


Fig. 3. (a) An AFM image of a CuInS₂ film on a quartz substrate. (b) A cross-sectional view of the surface corresponding to the line shown in Fig. 3a.

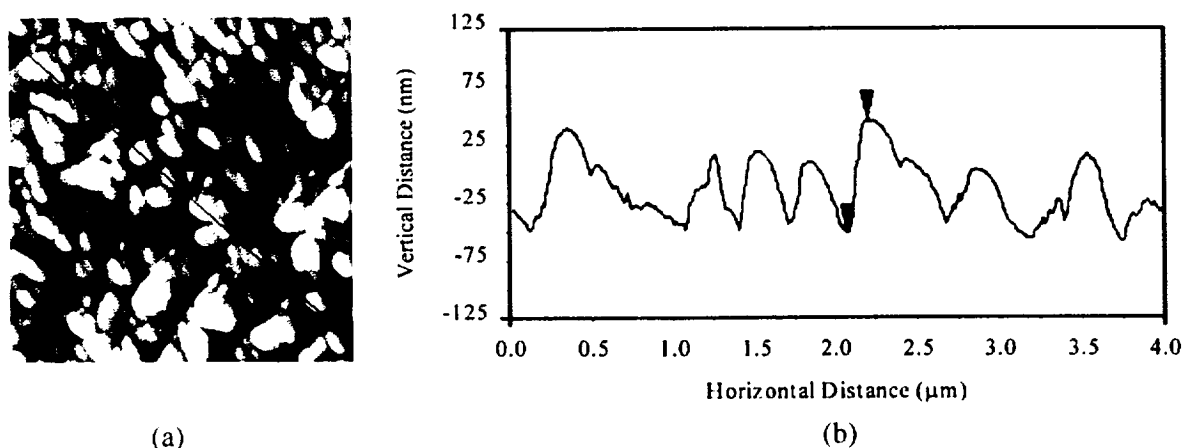


Fig. 4. (a) An STM image of a CuInS₂ film on a quartz substrate. (b) A cross-sectional view of the surface corresponding to the line shown in Fig. 4a.

are red-shifted by 32 and 35 cm⁻¹, respectively. We suspect the shift originates from anomalous dispersion in the reflectance measurements, where changes in the refractive index and extinction coefficient contribute. It would be desirable to perform a Kramers–Krönig transformation of the reflectance spectra, which would give reliable extinction and index spectra, but the transformation is impossible due to lack of spectral data below 200 cm⁻¹. The peak at 225 cm⁻¹ was not observed in previously reported spectra of CuInS₂ or CuIn₅S₈.

4. Conclusion

Spray chemical vapor deposition was used to deposit thin films of CuInS₂ from a single-source precursor. Rutherford backscattering measurements confirmed that these films were essentially stoichiometric, with a thickness of approximately 1 μm. An optical band-gap

of 1.44 eV was determined from optical absorption measurements. IR reflectance measurements identified phonon resonances at 225, 291 and 317 cm⁻¹. The latter frequencies are in reasonable agreement with

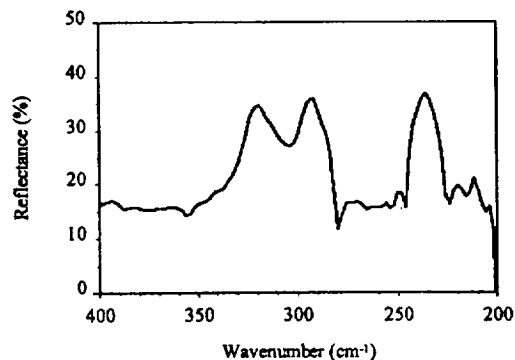


Fig. 5. Far-infrared reflectance spectrum of a CuInS₂ film on a quartz substrate.

previously reported values for the LO and TO modes of CuInS_2 .

Acknowledgements

We gratefully acknowledge the National Aeronautics and Space Administration for its support through grant NCC3-575, Consortium for Advancing Renewable Energy Technologies. Dr Harris was supported under NASA Grant NCC3-563 to Kent State University, Kent, Ohio.

References

- [1] Hedstrom J, Bodegard M, Kylner A, Stolt L, Schock H-W. Proc of the 23rd IEEE Photovoltaics Specialists Conf. New York: Institute of Electrical and Electronic Engineers, 1993:364.
- [2] Ermer J, Gay R, Pier D, Tarrant D. *J Vac Sci* 1993;A11:1888.
- [3] Grindle SP, Clark AH, Rezaie-Serej S, Falconer E, McNeily J, Kazmerski LL. *J Appl Phys* 1980;51:5464.
- [4] Schmid D, Ruckh M, Grunwals F, Schrock HW. *J Appl Phys* 1993;73:2902.
- [5] Stolt L, Hedström J, Kessler J, Ruckh M, Velthaus K-O, Schock H-W. *Appl Phys Lett* 1993;62:597.
- [6] Xiao H, Yang L-C, Rockett A. *J Appl Phys* 1994;76:1503.
- [7] Rockett and A, Birkmire RW. *J Appl Phys* 1991;70:R81.
- [8] Moller HJ. *Semiconductors for solar cells*. Boston: Artech House, 1993:33–36.
- [9] Hollingsworth JA, Buhro WE, Hepp AF, Jenkins PP, Stan MA. *Mat Res Symp Proc* 1998;495:171.
- [10] Stringfellow GB. *Phase equilibria diagrams*, volume IX. USA: The American Ceramic Society, 1992:272–273.
- [11] In Data in Science and Technology, *Semiconductors Other than Group IV Elements and III-V Compounds*, Ed. O. Madelung, Springer-Verlag, Berlin Heidelberg, 1992, pp. 57.
- [12] L.L. Kazmerski, P.J. Ireland, F.R. White, R.B. Cooper, 13th IEEE Photovoltaics Specialists Conf. New York, Institute of Electrical and Electronic Engineers, 1978, p. 185.



ELSEVIER

Solar Energy Materials & Solar Cells 63 (2000) 445–466

**Solar Energy Materials
& Solar Cells**

www.elsevier.com/locate/solmat

Electro-optical characterization and modeling of thin film CdS–CdTe heterojunction solar cells

V.P. Singh^{a,*}, D.L. Linam^a, D.W. Dils^a, J.C. McClure^b, G.B. Lush^a

^a*Department of Electrical and Computer Engineering, The University of Texas at El Paso, El Paso, TX, USA*

^b*Department of Materials Science and Engineering, The University of Texas at El Paso, El Paso, TX, USA*

Abstract

Optoelectronic characteristics of thin film CdTe–CdS solar cells fabricated at four different laboratories were measured and analyzed. Current versus voltage measurements revealed that, under one sun illumination, tunneling was the dominant current flow mechanism in all cells. Tunneling was also the dominant current flow mechanism in the dark for all types except P3 which exhibited a generation-recombination type current flow process in the dark. A theoretical model involving bulk traps in CdTe and a charged thin layer (T-layer) near the junction under forward bias and/or illumination was developed. The model is able to explain all significant features in the experimental results obtained from current versus voltage, and capacitance. © 2000 Elsevier Science B.V. All rights reserved.

Keywords: Solar cells; Thin film; Cadmium telluride

1. Introduction

Thin film CdS–CdTe solar cells are known to exhibit non-ideal effects which are not observed in single crystal cells like silicon. Crystalline cells, for example, exhibit “super-position” such that the current–voltage (I – V) characteristic under illumination has the same shape as the I – V characteristic in the dark, shifted only by a constant current value equal to the light generated short-circuit current (I_{sc}). The dark I – V and the light I – V curves, therefore, never cross each other. In thin film CdS–CdTe cells, on the other hand, the nature of the p–n junction itself seems to be altered by the incident solar illumination, causing the light I – V curve to cross the dark I – V curve at some

* Corresponding author. Present address: Department of Electrical Engineering, University of Kentucky, 453 Anderson Hall, Lexington, KY 40506-0046, USA..

forward bias voltage. This lack of super-position is often termed the “crossover” effect. It is important to understand these effects because they can lead to reduced cell efficiency and aging problems. Modeling of electron transport across the junction is needed for analyzing non-ideal effects and the loss mechanisms associated with them.

Many researchers have studied CdS–CdTe solar cells in the past [1–21] and reported on their characteristics and presented models. Some models are overly simplistic while others are primarily numerical models that provide little physical insight. We have investigated CdTe solar cells fabricated in four different laboratories using a variety of deposition techniques for CdS and CdTe. CdS layers of thickness 0.1–1 μm were deposited by chemical bath deposition (CBD), spray pyrolysis, or vacuum evaporation. CdTe layers of thickness 4–8 μm were deposited by close space sublimation (CSS), spray pyrolysis, vacuum evaporation, or electrochemical deposition. In this paper, we report the junction transport characteristics and develop a theoretical model to explain the cell behavior. The analytical model, presented in Section 3, provides physical insight into the junction behavior of CdS–CdTe cells in terms of a highly compensated π -CdTe layer and a high space charge layer next to CdS. Experimental results and discussion are given in Section 4.

2. Experimental procedures

Measurements were performed on four different CdS/CdTe cells fabricated at four different laboratories. All four cells had the device configuration shown in Fig. 1. The CdTe of cells P1, P2, and P3 was deposited by CSS, while cell P4 was deposited by spray pyrolysis.

All measurements were made with the cell mounted in a dewar vacuum system (Leybold #RB-210), which has a window for illumination. Five BNC connectors on the outside of the Dewar provided the connection for either current–voltage I – V or capacitance measurements. All cells were measured at 10 different temperatures ranging from 40 to 350 K (40, 50, 60, 75, 100, 150, 200, 250, 300, and 350 K). The temperature was controlled using a Leybold RW-3 helium refrigerant system, and a LakeShore 330 automatic temperature control unit.

Current–voltage measurements were made with an automatic tester that was controlled from a computer. Three different I – V curves were measured; dark, bias light, and one sun. Bias light measurements were made using a 15 W white light located 33 cm from the cell and off center by 30°. Capacitance–voltage and capacitance–frequency measurements were obtained using a Hewlett–Packard 4284A precision LCR meter and a Pentium-based computer. The voltage was varied in 0.1 V increments from –4.0 to 0.5 V at 1 MHz, –3.0 to 0.5 V at 100 kHz, –2.0 to 0.5 V at 10 kHz, and –1.0 to 0.5 V at 1 kHz. The voltage range was decreased for the lower frequencies because of a significant increase in loss current that precluded obtaining reliable data points. All of these capacitance measurements were performed in the dark and at various temperatures in the range of 40–350 K.

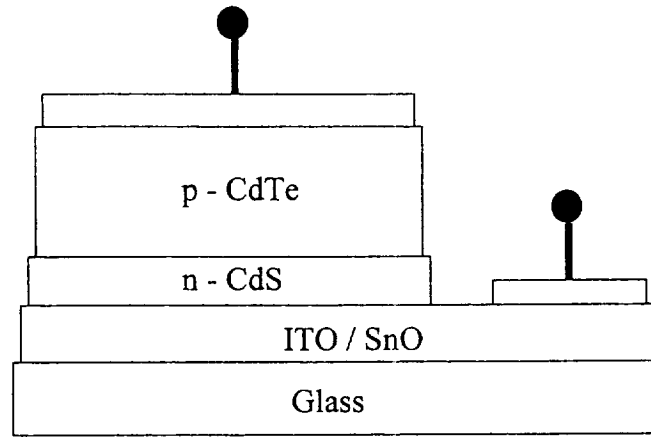


Fig. 1. Schematic of device structure for CdTe–CdS solar cell.

The raw data obtained were collated and analyzed in the graphing program. When computing J_0 and α from the I – V data the standard diode current equation was used:

$$J = J_0 \left[\exp \left(\frac{qV}{AkT} \right) - 1 \right] - J_L, \quad (1)$$

$$A = \frac{q}{kT\alpha}. \quad (2)$$

For analyzing capacitance data, the following equations were used [22,23]:

$$W(V) \mu\text{m} = \left(\frac{\epsilon_s}{C} \right) \times 1 \times 10^4, \quad (3)$$

$$N(W) \text{ cm}^{-3} = \frac{-2}{q\epsilon_s} \left(\frac{dV}{d(C^2)^{-1}} \right), \quad (4)$$

where J is the current density, V is the applied voltage, T is the temperature, W is the depletion layer width, C is the capacitance per unit area, ϵ_s is the dielectric constant of CdTe, $q = 1.6 \times 10^{-19} \text{ C}$, and N is the space charge density in CdTe.

3. Theory

3.1. Physical model

Based on the data from the current–voltage, capacitance–voltage, and capacitance–frequency measurements as functions of temperature and electroluminescence, spectral response and other electro-optical measurements, we model the

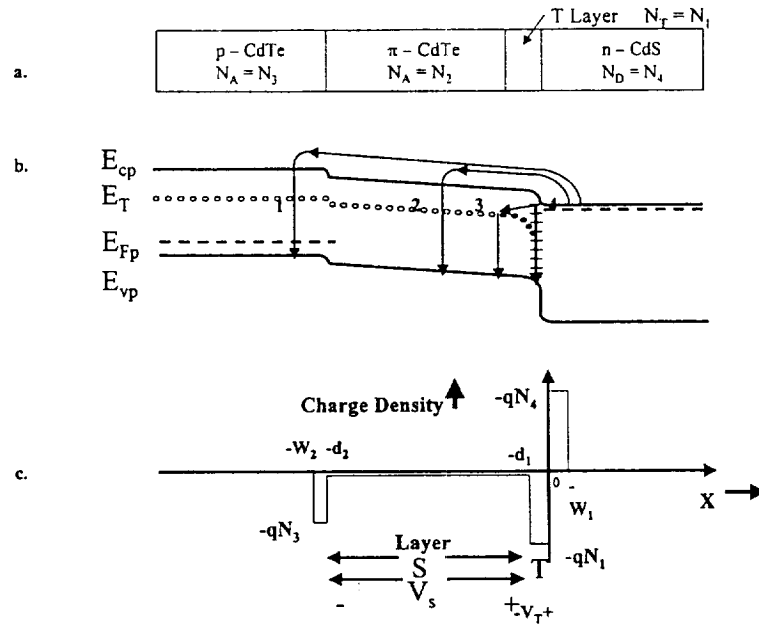


Fig. 2. Proposed model for the CdTe–CdS cell as a p– π –n device: (a) device configuration; (b) energy band diagram in forward bias; (c) space charge density diagram in forward bias.

CdTe–CdS solar cell as a p– π –n device with one or more bulk trap levels in the CdTe layer and interface states at the CdTe–CdS heterojunction (see Fig. 2(a)). Sketches of space charge distribution and band diagram under forward bias are shown in Figs. 2(b) and (c). A trap level of density N_T per cm^3 at an energy E_T above the valence band of CdTe is included. This, for example, could correspond to the trap level reported by Fortmann et al. [17,18] at 0.45 eV below the conduction band of CdTe. The bulk traps are assumed to be electrically neutral when empty. It should be noted that some of these trap levels in the vicinity of the heterojunction are below the Fermi level and are therefore negatively charged. We designate this negatively charged trap region as the T-layer. CdS is assumed to be much more conductive than CdTe. The built-in junction voltage, V_{bi} , is therefore, entirely on the CdTe side and is shared between the S-layer (the space charge layer to the left of T-layer) and the T-layer. It should be noted that only a minute fraction of the S-layer is in the p-CdTe. Most of the S-layer width lies in the i-CdTe layer. Note that we have termed the almost intrinsic π -CdTe layer as the i-layer. Contributions to the CdTe space charge come from the CdS–CdTe interface, the T-layer, the i-layer and the depleted portion of the p-type layer. Let V_s and V_T denote the voltage drops across the S-layer and the T-layer, respectively. In equilibrium, V_{bi} is sufficiently large that the hole population in the valence band of CdTe at the boundary of S and T layers is very small.

The I – V characteristics for cell P1 shown in Table 1 exhibit diode ideality factors (A factor) in excess of 2.0. The diode ideality factor in these cells is, in general, higher than

Table 1
 α and J_0 values under one sun illumination and in the dark, for cell P1

T (K)	$1/T$	α 1-sun	α dark	$\ln J_0$ 1-sun	$\ln J_0$ dark
40	0.025	4.94	2.63	−9.45	−10.57
50	0.020	5.95	2.56	−10.1	−10.50
60	0.016	5.23	2.65	−9.53	−10.56
75	0.013	5.57	2.62	−9.78	−10.54
100	0.010	5.50	2.67	−9.67	−10.53
150	0.0066	5.90	2.69	−9.79	−10.52
200	0.0050	5.19	2.85	−9.32	−10.57
250	0.0040	6.13	2.82	−9.99	−10.59
300	0.0033	6.84	3.08	−10.2	−10.60
350	0.0029	6.64	3.33	−9.98	−10.55

those for the CdTe–CdS cells from the Stanford group [10,12] where the value of A is typically less than 2.0. Also, α values are almost temperature independent in the dark as well as in the light. These data indicate that tunneling is an important junction transport mechanism in this cell. However, the zero-bias depletion layer width at room temperature is as high as 2.5 μm . The multistep tunneling through a wide depletion layer originally proposed by Riben and Feucht [24] for the Ge/GaAs heterojunction would require more than 70 tunneling steps for this cell [25]. A more likely mechanism is tunneling across a narrow, space charge layer near the CdS–CdTe interface, followed by recombination. In our model, we propose that such a layer could originate from the ionization of a deep trap level in CdTe. The existence of deep trap levels in this cell is suggested by the dispersion in junction capacitance (Fig. 3) and also by the rather slow drift in the I – V characteristic in the forward bias. Furthermore, the C – V characteristics of the device (Fig. 4) indicate the presence of an intrinsic layer at or near the CdS–CdTe junction. The $1/C^2$ versus V characteristics are similar to those seen for a p–i–n diode. The data of Fig. 4 can be split into two regions. For large reverse bias values, the region on the left shows little variation in capacitance versus voltage. This corresponds to a high space charge density p-region, away from the n-CdS. As we approach the zero bias (region on the right), the capacitance increases sharply with increasing voltage; this is symptomatic of a low space charge density (intrinsic or i-layer) closer to the n-CdS. In fact this i-layer may be on the CdS side or the CdTe side of the junction, or it may straddle the junction. It is hard to separate the effects of these three possibilities from the data of Fig. 4. Here we assume the i-layer to be on CdTe side and model the cell as a p–i–n device sketched in Fig. 2(a).

Current across the junction in these devices can follow four paths (see Fig. 2(b)). Path 1 is the diffusion current. Path 2 is the generation-recombination current. Path 3 involves tunneling between CdS conduction band and empty trap levels followed by hole capture by the trap. Path 4 is recombination via interface states. At zero bias, V_a (Fig. 2(c)) is large so that path 2, and path 1 to some extent, is limited by the relatively small hole supply in the i-layer. Also, the tunneling current and the interface

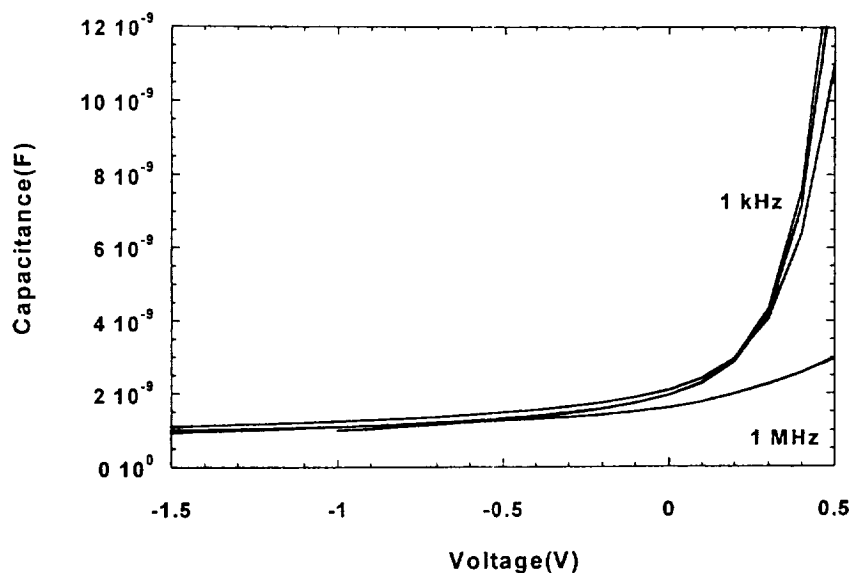


Fig. 3. Capacitance–voltage response of cell P1 at 300 K at various frequencies in the 1 kHz to 1 MHz range.

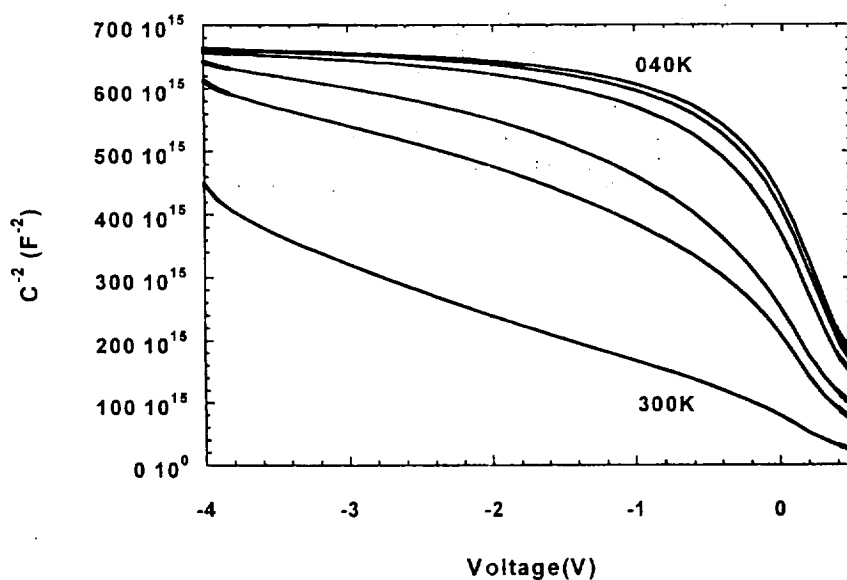


Fig. 4. $1/C^2$ versus voltage at 40, 50, 100, 150, 200, 250, and 300 K for cell P1.

recombination are small because hole population at the i–T interface and the CdS–CdTe interface is inadequate. Application of a forward bias, however, results not only in a reduction in the total barrier potential but also in an increase in the width of the T-layer (Fig. 2(c)). This is caused by a larger number of trap levels falling

below E_{Fn} . The result is that the ratio V_T/V_a is now higher than it was in equilibrium. There is a decrease in V_a , due to both forward bias decreasing the total barrier from V_{bi} to $V_{bi}-V_F$, and due to V_T absorbing a larger proportion of $V_{bi}-V_F$. This reduces V_s (see Fig. 2(c)) and makes a large number of holes available at the i–T interface. Note that the hole population at the i–T interface is equal to $N_3 e^{(-V_s/kT)}$. The tunneling current path now becomes significant, as does the depletion layer recombination current. Interface recombination current will also be enhanced. The effective value of the diode reverse saturation current density J_0 thus increases with forward bias.

Another prediction of this model is that if the cell is left in the forward biased state for an extended period of time (seconds, minutes, hours), the trap population continues to alter slowly (slow traps) so that the width of the T-layer continues to increase slowly. This results in more holes becoming available in the valance band of CdTe at the i–T layer interface. Consequently, the forward “loss” current (or J_0) continues to increase, as observed experimentally. Also, direct recombination of electrons injected into the conduction band of CdTe and the holes at the i–T interface in CdTe is enhanced. This leads to enhanced electroluminescence, as observed experimentally [26].

When a forward bias is applied to the solar cell, the quasi-Fermi level for electrons (E_{Fn}) rises above the quasi-Fermi level for holes (E_{Fp}). Some of the trap levels (initially empty and neutral) now fall below (in energy) the rising E_{Fn} . These traps now capture an electron, which was either (a) injected into the conduction band of CdTe from the conduction band of CdS or, more likely, (b) tunnel injected into the trap level directly from the conduction band of CdS. The latter mechanism is preferred because of the close physical vicinity between the CdS conduction band and the right end of the T-layer. Once the electron has been injected into a trap on the right end of the T-layer, it can (a) “hop” to another empty trap level to its left which also lies below E_{Fn} , thus increasing the width of the T-layer, (b) relax down to the valance band of CdTe, thus capturing a hole. After the process (a) or (b) is completed, a new electron can be tunnel injected from the CdS conduction band at the right end of the T-layer.

The hole in the valance band of CdTe in the T-layer, captured by the trap, is resupplied from the p-CdTe at the left end of the π -CdTe (or i-CdTe). Thus, the current in most of the π -layer is due to holes diffusing from the p-CdTe into π -CdTe against a potential barrier (V_s). The current in the T-layer is due to recombination of electrons and holes. The current between the CdS and the T-layer is due to the injection of electrons by tunneling. If path 3 were the only forward current flow path (assuming paths 1, 2 and 4 to be negligible), then in steady state these three currents will be equal. In general, the total forward current will be limited by how many holes can be supplied by p-CdTe to the π -CdTe, or by the concentration of holes in CdTe at the boundary between the π -layer and T-layer. This concentration is determined by the value of V_s because V_s is the barrier to diffusion of holes from the p-CdTe to the right end of π -CdTe. The value of V_s is, in turn, dependent upon the total negative charge in the T-layer and the forward bias applied. The higher the forward bias, the wider the T-layer, smaller the V_s and larger the hole supply to the T-layer, leading to

an increase in forward current with forward bias which is super-exponential. Application of forward bias (V_F) in this manner alters the nature of the heterojunction leading to a non-constant effective reverse saturation current (J_0). Thus, unlike the traditional single crystal Si or GaAs diodes, J_0 increases with V_F .

Because the trap levels (E_T) in CdTe are relatively deep, they are quite “slow” to reach a steady-state and/or equilibrium occupancy. It may take seconds, minutes or hours for the electron population in these traps to arrive at a steady-state value. As a result, when a fixed, high forward bias is applied to the solar cell for a long time, the forward current continues to drift to higher and higher values.

Exposing the solar cell to optical radiation or sunlight has an effect on the electron occupancy of trap levels, which is similar to the application of a forward bias. As a result, the effective reverse saturation current (J_0) is dependent not only on V_F , but also on the intensity and wavelength of the incident optical radiation. Thus it is that, (i) measured J_0 in light is higher than in the dark, (ii) measured ΔV_{OC} and ΔI_{SC} are dependent upon V_F , intensity of bias light, and the wavelength of bias light [1], (iii) measured electroluminescence output (caused by the recombination of electrons injected into the conduction band of CdS and the holes in the valance band of CdTe in or near the T-layer) is dependent upon V_F and drifts with time [26].

If, by improved processing, the bulk traps in CdTe are reduced or made shallower (closer to the conduction band in CdTe), then the charge in the T-layer will be reduced. Effects such as tunnel injection and the variations in J_0 discussed above will be reduced, current paths 1 and 2 will become more dominant, and the value of α will tend to increase (towards a value of 20 or 40 at room temperature) and become dependent on temperature. As a result, J_0 will be reduced and the open-circuit voltage and efficiency of the cell will be higher.

3.2. Charge, field, and carrier concentration

Expressions for field strength, charge, and carrier concentrations in the p, π , and T layers of CdTe were presented earlier by Singh et al. [1] and by Makwana [27], and are reproduced here for convenience. Also, more detailed explanations for some equations have been added and typographical errors from Eqs. (2)–(6) of Ref. [1] have been removed.

The space charge distribution sketched in Fig. 2 is used to calculate the hole concentration at the S–T interface as a function of forward bias. From Fig. 2(b), the junction voltage in equilibrium is seen to be

$$V_{bi} = \frac{E_{gp}}{q} - \frac{kT}{q} \left\{ \ln \left(\frac{N_v}{N_3} \right) - \ln \left(\frac{N_c}{N_4} \right) \right\}, \quad (5)$$

where N_v is the effective density of states for the valence band of CdTe, and N_c is the effective density of states for the conduction band of CdS. The electric field distribution in the space charge layer of Fig. 2 is given by the following Eqs. (6)–(12).

For the p-CdTe region described as $-W_2 < x < -d_2$ (see Fig. 2(c)), integrating space charge to obtain the electric field one obtains

$$E(x) = -\frac{qN_3(x + W_2)}{\epsilon_p} \quad (6)$$

Letting $x = -d_2$ in Eq. (6) one obtains

$$E(-d_2) = E_2 = -\frac{qN_3(W_2 - d_2)}{\epsilon_p} \quad (7)$$

For the T-layer, described in Fig. 2(c) as $-d_2 < x < -d_1$, the space charge density is qN_2 , and the electric field is given by

$$E(x) = E_2 - \frac{qN_2(x + d_2)}{\epsilon_p} \quad (8)$$

Letting $x = -d_1$ in Eq. (8), the result is

$$E(-d_1) = E_1 = E_2 - \frac{qN_2(d_2 - d_1)}{\epsilon_p} \quad (9)$$

Similarly, for the T-layer described in Fig. 2(c),

$$E(x) = E_1 - \frac{qN_1}{\epsilon_p(x + d_1)} \quad \text{for } -d_1 < x < 0. \quad (10)$$

Letting $x = 0$ in Eq. (10) one obtains

$$E(0^-) = E_{01} = E_1 - \frac{qN_1 d_1}{\epsilon_p} \quad (11)$$

Also from Gauss' Law, $\epsilon_n E_{02} - \epsilon_p E_{01} = Q_i$, where Q_i (C cm^{-2}) is the interface charge density, and E_{02} is the electric field at $x = 0^+$. At $V_F = 0$

$$Q_i(0) = -qN_1 \frac{E_F(0) - E_v(0)}{E_g} \text{ C cm}^{-2}, \quad (12)$$

where $E_F(0)$ is the Fermi level and $E_v(0)$ is the valence band edge of CdTe at $x = 0$, E_g is the energy band gap of CdTe, and N_1 is the total number of interface states (assumed to be uniformly distributed over the band gap of CdTe, at $x = 0$). Here we have assumed that the interface states are neutral when empty. Furthermore, we have assumed that all states above $E_F(0)$ are empty, and all below $E_F(0)$ are occupied.

Application of forward bias splits the Fermi level E_F into quasi-Fermi levels for holes (E_{Fp}) and for electrons (E_{Fn}). The energy difference between E_{Fn} and E_{Fp} at the interface is qV_F . The interface charge, Q_i , is now given by

$$Q_i(V_F) = -\frac{qN_1}{E_g}(E_F(0) - E_v(0) - qV_F). \quad (13)$$

Using Gauss's law and Eq. (13) we get

$$E_{02} = \frac{1}{\epsilon_n} \left(\epsilon_p E_{01} - qN_1 \frac{E_F(0) - E_v(0) - qV_F}{E_g} \right). \quad (14)$$

From Fig. 2, it is evident by inspection that

$$E_F(0) - E_v(0) = E_g - \Delta E_c + \frac{qE_{02}W_1}{2} - q\delta_n - qV_F. \quad (15)$$

To write Eq. (15), we start at the conduction band of CdTe at the interface ($x = 0^+$), come down by ΔE_c , come down by $qE_{02}W_1/2$ which is the band bending in the CdS, come down by $q\delta_n$ to reach E_{Fn} and then come down by qV_F to reach E_{Fp} . Note that E_{02} is a negative number, and

$$\delta_n = \frac{E_{cn} - E_{Fn}}{q} = \frac{kT}{q} \ln \left(\frac{N_c}{N_D} \right). \quad (16)$$

N_D is the donor concentration in CdS, and ΔE_c is the difference between the electron affinities of CdS and CdTe.

On the CdS side of the junction, the space charge density is qN_4 and the field is given by

$$E(x) = E_{02} + \frac{qN_4x}{\epsilon_n} \quad \text{for } 0 < x < W_1. \quad (17)$$

The total voltage drop due to space charge at the junction is given as

$$V_{sc} = ((V_{bi} - V_f) - \Delta E_c/q). \quad (18)$$

Integrating the electric field, V_{sc} is found to be

$$V_{sc} = -0.5\{E_2(W_2 - d_2) + (E_1 + E_2)(d_2 - d_1) + (E_{01} + E_1)d_1 + E_{02}W_1\}. \quad (19)$$

The condition of global space charge neutrality requires that

$$qN_3(W_2 - d_2) + qN_2(d_2 - d_1) + qN_1d_1 - Q_i = qN_4W_1. \quad (20)$$

Since $x = -d_1$ is the point at which E_T crosses E_{Fn} , an examination of Fig. 2 yields

$$\delta_n + \frac{\Delta E_c}{q} - \frac{E_{02}W_1}{2} - \frac{(E_{01} + E_1)d_1}{2} = \frac{E_{cp} - E_T}{q} = 0.45V. \quad (21)$$

Further, from Fig. 2 we see that

$$V_1(-d_1) = \{-0.5\{E_2(W_2 - d_2) + (E_1 + E_2)(d_2 - d_1)\}\}. \quad (22)$$

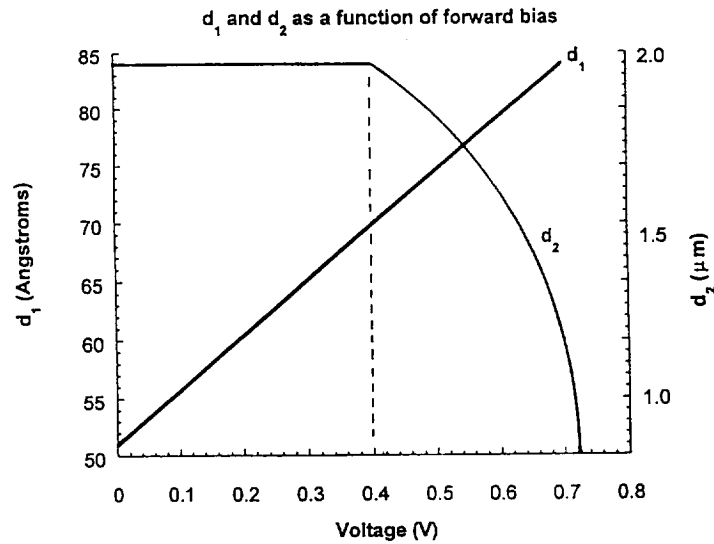


Fig. 5. Effect of forward bias on (a) the width of the T-layer and (b) the width of the i-CdTe layer.

The hole concentration at $x = -d_1$ is given by

$$p_1 = p(\text{at } x = d_1) = p_p \exp\left(\frac{-qV_1}{kT}\right), \quad (23)$$

where p_p is the free hole concentration in the bulk CdTe which is also the free hole concentration at $x = -W_2$.

When there is no interface charge at the CdS–CdTe interface ($N_1 = 0$), the junction capacitance can be expressed as [23]

$$C = \frac{A\epsilon_p}{\left\{ \frac{2\epsilon_p(V_{bi} - V_F)}{q(N_2 + N_3)} + \frac{N_3 d_2^2}{N_2 + N_3} - \frac{N_1 d_1^2}{N_2 + N_3} \right\}^{0.5}}. \quad (24)$$

For known or assigned values of W_2 , E_i , N_1 and carrier concentrations N_1 , N_2 , N_3 and N_4 , one can use Eqs. (5)–(21) to evaluate d_1 , d_2 , W_1 , E_1 , E_2 , E_{01} and E_{02} . Eqs. (22) and (23) are then used for calculating the hole concentration at the S–T interface. Results of such a calculation for $W_2 = 2.0 \mu\text{m}$, $E_T = 0.45 \text{ eV}$, $N_1 = 5 \times 10^{11} \text{ cm}^{-2}$, $N_1 = 5 \times 10^{17} \text{ cm}^{-3}$, $N_2 = 1 \times 10^{14} \text{ cm}^{-3}$, $N_3 = 6 \times 10^{15} \text{ cm}^{-3}$ and $N_4 = 1 \times 10^{17} \text{ cm}^{-3}$ are shown in Figs. 5 and 6. We note that in Fig. 5, as V_F increases from 0.0 to 0.44 V, there is an increase in d_2 with a resulting reduction of space charge remaining in the p-CdTe layer; at $V_F = 0.44 \text{ V}$, $d_2 = W$ and the only CdTe space charge is in the i-CdTe layer and the T-layer. A further increase in V_F results in a drastic reduction in depletion layer width, d_2 . For $V_F = 0.68 \text{ V}$, d_2 has decreased all the way down to d_1 . At this point the entire CdTe space charge layer is in the T-layer. A further increase in V_F will result in a reduction of d_1 itself. Thus, 85 Å represents the maximum width of

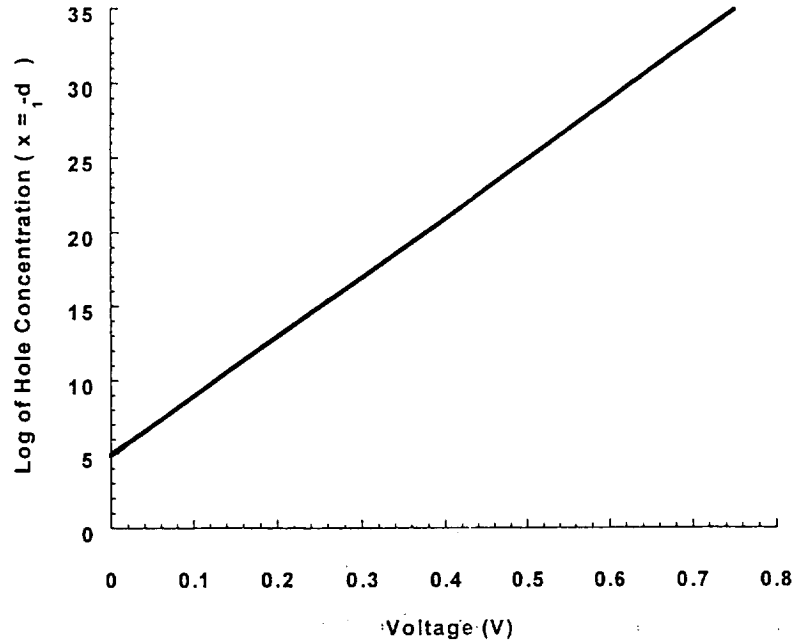


Fig. 6. Logarithm of hole concentration at $x = -d_1$ as a function of forward bias voltage; computer simulation.

the T-layer. Fig. 6 shows that the hole concentration at the S-T interface increases exponentially with increasing V_F . Therefore, one may expect a roughly exponential increase in the tunneling component of loss current.

3.3. Junction currents

3.3.1. Computation of the tunnel-recombination current (path 3)

If N_t is the density of traps per cm^3 then from Ref. [28], n_t , the density of electrons in the trap levels in the T-layer is given as

$$n_t = N_t P_{\text{occ}}, \quad (25)$$

where P_{occ} is the occupation probability given by

$$P_{\text{occ}} = \frac{1}{1 + \exp((E_t - E_{Fn})/kT)} \cong \exp\left(\frac{E_{Fn} - E_t}{kT}\right), \quad (26)$$

when $E_{Fn} \gg E_t$ with the constraint of $n_t \leq N_t$. The density of unoccupied traps ($p_t = N_t - n_t$) is given by

$$p_t = N_t(1 - P_{\text{occ}}) = N_t \frac{\exp((E_t - E_{Fn})/kT)}{1 + \exp((E_t - E_{Fn})/kT)} \quad (27)$$

and the tunnel current (I_t) due to tunneling of electrons from the conduction band of CdS to the unoccupied trap levels on the right end of the T-layer is given by [24,29]

$$I_t = B p_i \exp \left[-4(2m_i q)^{1/2} \left(\frac{V_d - k_2 V}{3\hbar H_0} \right) \right], \quad (28)$$

where

$$H_0 = \left(\frac{2qN_A}{\epsilon_s} \right)^{1/2}. \quad (29)$$

The junction potential barrier is given by

$$qV_d = E_{gt} + \Delta E_v - \delta_n - \delta_p - qV_F, \quad (30)$$

which is also equivalent to the barrier potential for tunneling where V_F is the applied forward bias, E_{gt} is the bandgap of CdTe, $\delta_n = E_c - E_{Fn}$ (in CdS), and $\delta_p = E_{Fp} - E_v$ (in CdTe).

In writing Eqs. (28) and (29), we have assumed that there are plenty of electrons available in the CdS conduction band. I_T is thus limited by the tunneling and by the number of available states (p_i) which are the tunnel destinations. Of course p_i cannot exceed N_t .

Current due to capture of holes by the electrons trapped in the T-layer is given by [30]

$$J_{rec} = \int_0^{W_T} q n_i p(0^-) \sigma_p \mathcal{G}_{th} dx, \quad (31)$$

which is the rate of hole capture by traps in the T-layer. Furthermore,

$$\int_0^{W_T} q p(0^-) \sigma_p \mathcal{G}_{th} N_T \frac{dx}{1 + \exp((E_t - E_{Fn})/kT)}, \quad (32)$$

where σ_p is the capture cross section of holes, W_t is the width of the T-layer, and \mathcal{G}_{th} is the thermal velocity. In steady state,

$$J_{rec} = J_{tunnel}. \quad (33)$$

The value of the tunnel recombination current (path 3) is limited by the lesser of currents given by Eqs. (31) and (32). Eq. (33) can be used to evaluate $p(0^-)$ if n_i , σ_p , E_{Fn} , etc. are known.

3.3.2. Current path 1: Diffusion current

Diffusion current can be expressed as [31]

$$J = J_0 [e^{(qV/AkT)} - 1]. \quad (34)$$

3.3.3. Current Path 2: Generation-recombination current

The recombination current in the depletion layer in CdTe is given by [32]

$$J_{\text{rec}} = \int_0^{W_{\text{dep}}} qU \, dx, \quad (35)$$

where

$$U = \frac{\sigma_p \sigma_n g_{\text{th}} N_t n_i^2 \left(\exp\left(\frac{qV}{kT}\right) - 1 \right)}{\sigma_n \left[n + n_i \exp\left(\frac{E_t - E_i}{kT}\right) \right] + \sigma_p \left[p + n_i \exp\left(\frac{E_i - E_t}{kT}\right) \right]}. \quad (35a)$$

Under the assumption that $E_i = E_t$ and $\varepsilon_n = \varepsilon_p$ Eq. (35a) reduces to

$$U = \frac{\sigma_n g_{\text{th}} N_t n_i^2 (e^{qV/kT} - 1)}{n + p + 2n_i} \quad (36)$$

and assuming that $V \gg kt/q$, Eqs. (35) and (36), after simplification [32], give

$$J_{\text{rec}} = \frac{qW_{\text{dep}} n_i}{2T_r} \exp\left(\frac{qV}{2kT}\right), \quad (37)$$

where

$$T_r = \frac{1}{(\sigma g_{\text{th}} N_t)} \quad (38)$$

and W_{dep} is the depletion layer width in CdTe.

3.3.4. Current path 4: Interface recombination

The interface recombination current due to electrons from CdS side and holes from the CdTe side is given by [33]

$$J_n = q\sigma_n v_{\text{th}} N_1 \left(n(0^+) (E_c(0^+) - E_{\text{Fp}}) - \frac{n_0(0^+) (E_c(0^+) - E_{\text{Fp}}) (E_{\text{Fp}} - E_v(0^-))}{E_{\text{F0}} - E_v(0^-)} \right) \quad (39)$$

and

$$J_p = q\sigma_p v_{\text{th}} N_1 \left((p(0^-) (E_{\text{Fp}} - E_v(0^-)) - \frac{p_0(0^-) (E_{\text{F0}} - E_v(0^-)) (E_c(0^+) - E_{\text{Fp}})}{E_c(0^+) - E_{\text{F0}}}) \right), \quad (40)$$

where σ_n is the electron capture cross section, σ_p is the hole capture cross section, v_{th} is the electron thermal velocity, E_{F0} is the equilibrium value of the fermi level given by

$$E_{\text{F0}} = E_{\text{Fp}} + qV_{\text{F}}. \quad (41)$$

Free electron concentration on the CdS side of the interface is given by

$$n(0^+) = N_D e^{-qV_1/kT}. \quad (42)$$

Free hole concentration on the CdTe side of the interface is given by

$$p(0^-) = N_A e^{-qV_1/kT}, \quad (43)$$

where

$$V_2 = -0.5(E_{02}W_1) \quad (44)$$

and

$$V_1 = V_{sc} = -0.5(E_2(W_2 - d_2) + (E_1 + E_2)(d_2 - d_1) + (E_{01} + E_1)d_1 + E_{02}W_1). \quad (45)$$

Additionally, the equilibrium value of $n(0^+)$ is given by

$$n_0(0^+) = N_D e^{qV_{20}/kT}. \quad (46)$$

The equilibrium value of $p(0^-)$ is given by

$$p_0(0^-) = N_A e^{-qV_{10}/kT}, \quad (47)$$

where

$$V_{20} = \text{initial barrier height} = -0.5(E_{020}W_{10}) \quad (48)$$

and

$$V_{10} = V_{sc0} = -0.5 \left(E_{20}(W_{20} - d_{20}) + (E_{10} + E_{20})(d_{20} - d_{10}) + (E_{010} + E_{10})d_{10} + E_{020}W_{10} \right). \quad (49)$$

The values E_{10} , E_{20} , E_{010} , E_{020} , d_{10} , d_{20} , W_{10} , V_{20} , V_{sc0} , and V_{10} are at zero bias. Eqs. (39) and (40) are solved using Eqs. (41)–(49). Since the interface-recombination current is largely dependent on the availability of holes at the CdS/CdTe interface, the net interface-recombination current can be approximated as $J_{rec} \approx J_p$.

4. Results and discussion

The current–voltage characteristics of cell P1 at various temperatures are shown in Fig. 7 in the dark and Fig. 8 under one-sun illumination. The efficiency of this cell varied from 12% at 300 K to 14% at 40 K. Values of J_0 and α that were obtained from the data are tabulated in Table 1 and are plotted versus $1/T$ in Figs. 9 and 10.

Capacitance–voltage data at four different frequencies are plotted in Fig. 3. Note that the zero bias capacitance increases as the measurement frequency is reduced.

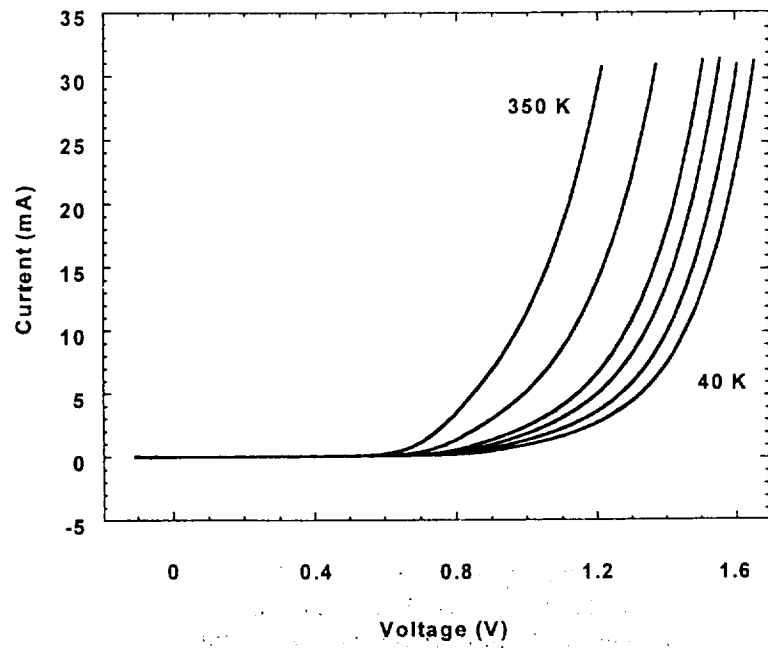


Fig. 7. Current-voltage response of cell P1 in the dark at 40, 200, 250, 300, and 350 K.

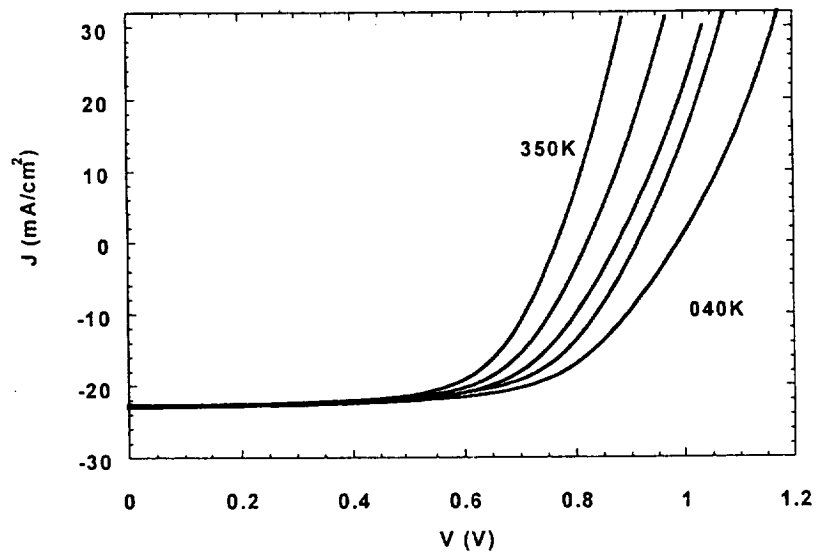


Fig. 8. Current-voltage response of cell P1 under one sun illumination at 40, 200, 250, 300, and 350 K.

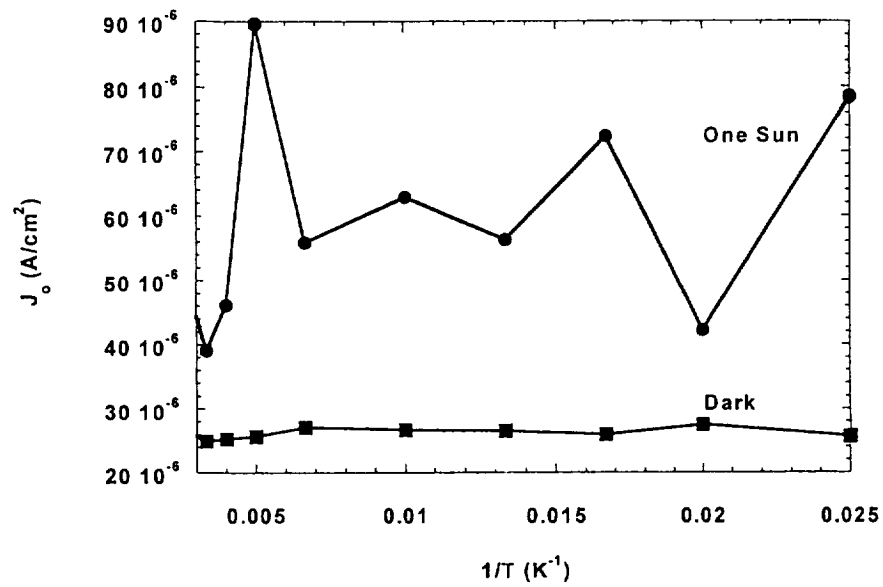


Fig. 9. Diode reverse saturation current (j_0) versus $1/T$; under one sun illumination and in the dark for cell P1.

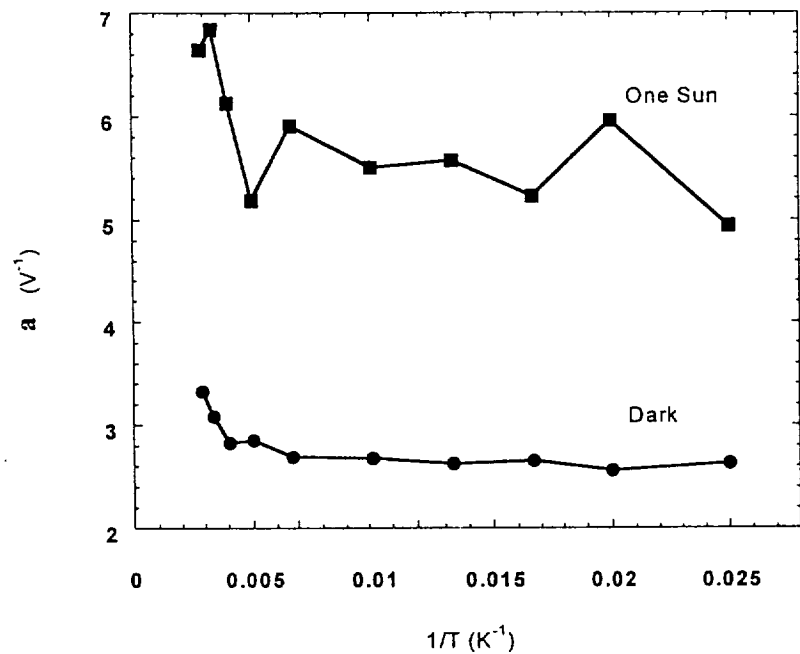


Fig. 10. α versus $1/T$; under one sun illumination and in the dark; cell P1.

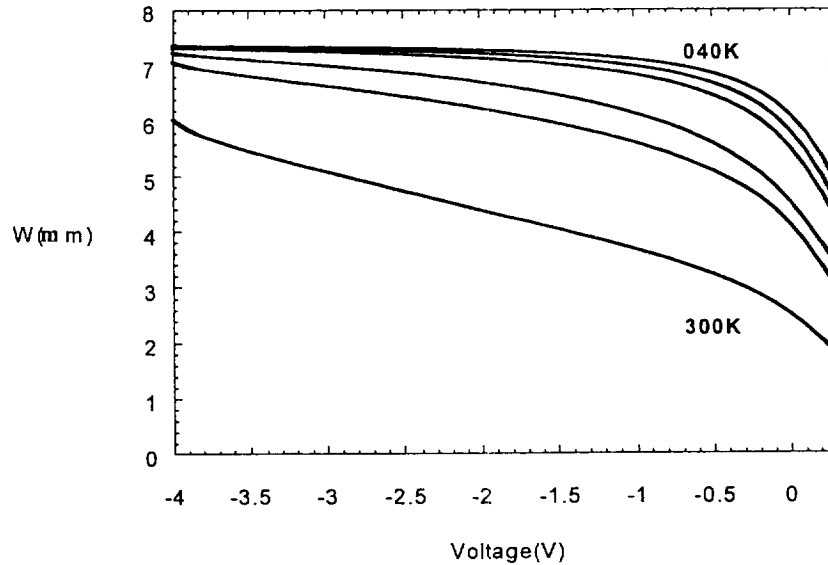


Fig. 11. Depletion layer width (W) as a function of voltage and temperature, cell P1 (40, 100, 150, 200, 250, and 300 K).

The depletion layer width (W) as a function of voltage and temperature is plotted in Fig. 11. W was deduced from the data using

$$W = \frac{A\epsilon_s}{C}, \quad (50)$$

where A is the area, C is the capacitance and ϵ_s the dielectric constant. Fig. 4 shows the plots of $1/C^2$ versus V at different temperatures. Space charge density (N) was computed from the data of Fig. 4 and is plotted against W in Fig. 12.

We observe from Fig. 12 that at 150 K the value of the effective carrier concentration (N) in CdTe is close to 10^{15} cm^{-3} near the surface, which is about $7.2 \mu\text{m}$ away from the CdTe–CdS junction. The value of N is much lower (in the $5 \times 10^{13} \text{ cm}^{-3}$ range) in the CdTe region which is $4.5\text{--}7 \mu\text{m}$ away from the CdTe–CdS junction. Thus, the CdTe layer appears to be p-type near the surface and π -type (low doped) between the surface and the CdTe–CdS junction, as modeled in Section 3 above.

From Table 1 and Fig. 10 we see that under one sun illumination, the value of α for the CdTe–CdS diode is in the 4.9–6.6 range and is practically temperature independent. In the dark, α is in the 2.5–3.3 range and again practically temperature independent. Temperature independence suggests that tunneling is the dominant current flow mechanism in this diode. In other words, the current path 3 in the model presented in Section 3 is the preferred path for electron flow across the junction. Note that the value of J_0 under illumination is substantially higher than its value in the dark (Fig. 9). We attribute this to the widening of the T-layer (see Section 3 and Fig. 2) which increases the supply of holes in CdTe in the T-layer and thus increases the tunneling-recombination current.

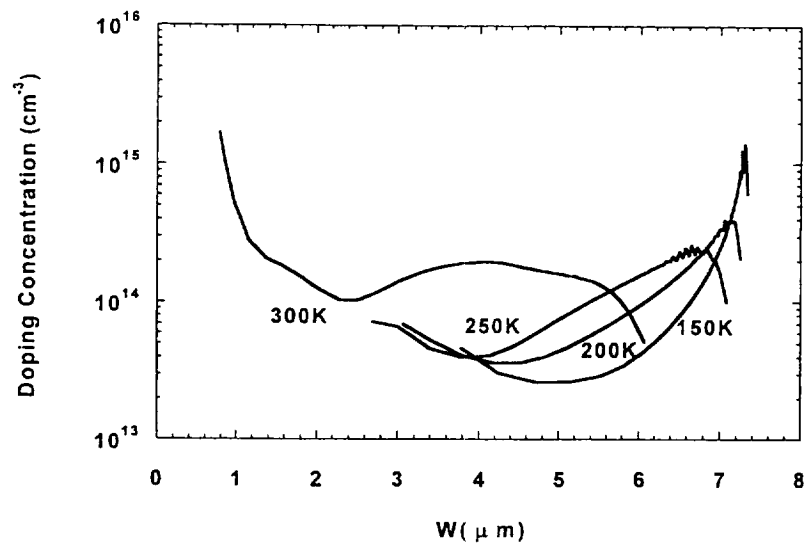


Fig. 12. Effective doping concentration (N) in CdTe as a function of distance; cell P1.

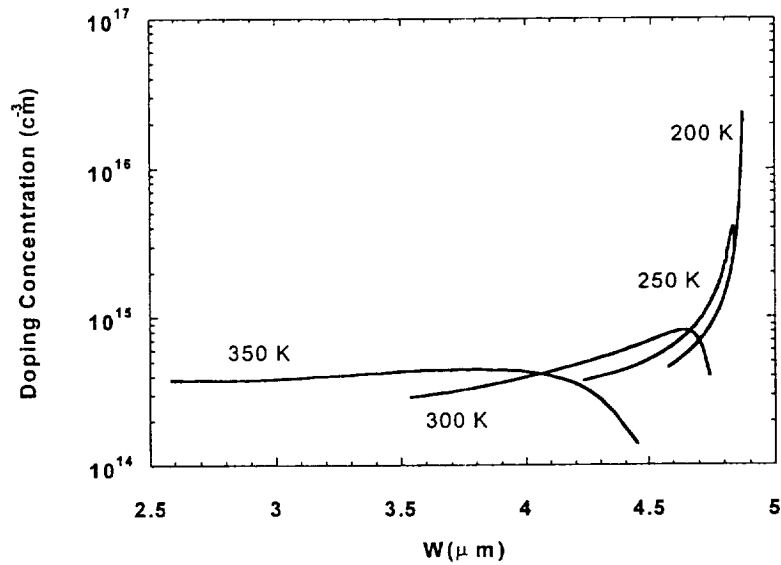
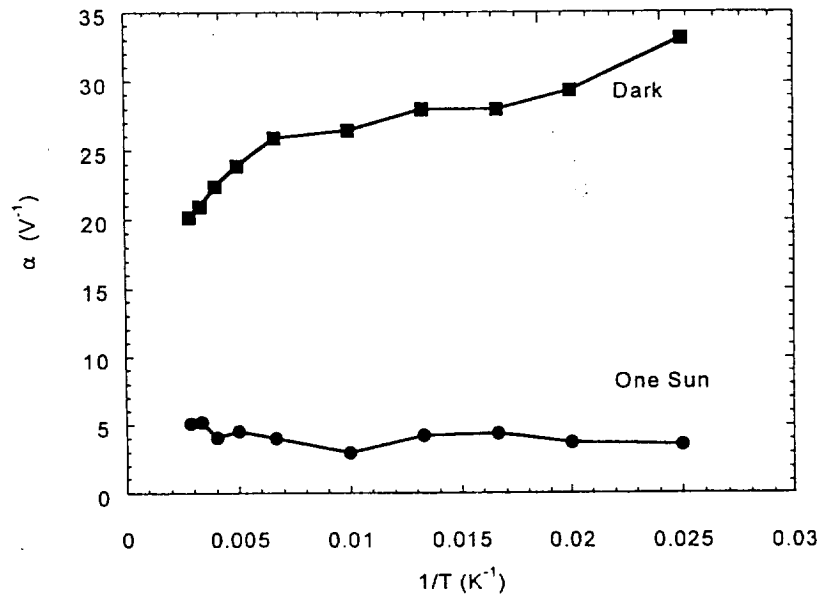
The frequency dependence of capacitance seen in Fig. 3 is attributed to charge trapped in the bulk trap E_T (see Fig. 2) and to the interface states, which tend to be relatively “slow”. A substantial decrease in the depletion layer width at higher temperature, seen in Fig. 11, indicates that thermal excitation of carriers between the traps and energy bands in CdTe plays an important role in the junction behavior in these solar cells.

The four types of CdTe–CdS solar cells we tested were fabricated at four different laboratories and varied in the details of fabrication processing. Nevertheless, capacitance measurement results were similar for all of them; they all showed a p-type CdTe near the surface and n -type CdTe in the rest of the CdTe layer. For example, Fig. 13 shows the N versus W results for cell P2. However, α values for P2 were larger. At room temperature α was 16 in the dark and 5.7 under one sun illumination. In the dark, J_0 was $1.3 \times 10^{-9} \text{ A cm}^{-2}$ and increased to $6.6 \times 10^{-5} \text{ A cm}^{-2}$ under one sun illumination.

Cell P3 exhibited a temperature-independent α value of approximately 5 under one sun illumination and a temperature-dependent α of 20 and higher in the dark (see Fig. 14). Thus, in this cell generation-recombination current (path 2 in Fig. 2, Section 3) appears to be dominant in the dark. Under one sun illumination, tunneling is dominant as in other cells. This is attributed to the widening of the T-layer when the cell is illuminated; exposure to sunlight creates a forward bias across the CdTe–CdS junction, leading to the opening of the tunneling current path 3.

5. Conclusions

Electro-optical characterization of four types of thin film CdTe–CdS solar cells made at four different laboratories revealed that their capacitance–voltage and

Fig. 13. Effective doping concentration (N) in CdTe as a function of distance; cell P2.Fig. 14. α versus $1/T$; under one sun illumination and in the dark; cell P3.

capacitance–frequency behaviors were similar in nature. All showed a p– π –n type of structure; CdTe carrier concentration was relatively high ($\sim 10^{15} \text{ cm}^{-3}$) near the surface and low ($\sim 2 \times 10^{13} \text{ cm}^{-3}$) between the surface and the CdTe–CdS junction.

Current–voltage measurements revealed that under one sun illumination tunneling was the dominant current flow mechanism in all cells. Tunneling was also the dominant current flow mechanism in the dark for all types except P3, which exhibited a generation-recombination type current flow process in the dark.

A theoretical model involving bulk traps in CdTe and a highly charged thin layer (T-layer) near the junction under forward bias and/or illumination was developed. The model is able to qualitatively explain all significant features in the experimental results obtained from current–voltage, and capacitance. It is planned next to use Eqs. (5)–(49) of Section 3 to calculate the contributions of various current paths to the total junction current and compare the theoretical current to the experimentally measured current under various voltage bias and illumination intensity values.

Acknowledgements

Thanks are due to NASA-BMDO for partial support in the funding of research performed (Grant # 26120379). We are grateful to National Renewable Energy Laboratory, Golden Photon Inc., University of South Florida, and First Solar Inc. for providing experimental solar cell samples. Thanks are due to Daniel Doran for helping with the measurement setup.

References

- [1] V.P. Singh, H. Brafman, J. Makwana, *Sol. Cells* 31 (1991) 23.
- [2] V.P. Singh, O.M. Erickson, J.H. Chao, *J. Appl. Phys.* 78 (1995) 4538.
- [3] S.P. Albright, B. Ackerman, J.F. Jordan, *IEEE Trans. Electron Dev.* 37 (1990) 434.
- [4] V.P. Singh, R.H. Kenny, J.C. McClure, S.P. Albright, B. Ackerman, J.F. Jordan, *Proceedings of the 19th Photovoltaic Specialists' Conference, IEEE, New York, 1987*, pp. 216–221.
- [5] S.P. Albright, V.P. Singh, J.F. Jordan, *Sol. Cells* 24 (1988) 43.
- [6] J.F. Jordan, S.P. Albright, *Sol. Cells* 23 (1988) 107.
- [7] V.P. Singh, J.C. McClure, G.B. Lush, W. Wang, X. Wang, G.W. Thompson, *Sol. Energy Mater. Sol. Cells* 59 (1999) 145–161.
- [8] J. Britt, C. Ferekides, *Appl. Phys. Lett.* 62 (22) (1993) 2851.
- [9] H.C. Chou et al., *Mater. Chem. Phys.* 43 (1996) 178.
- [10] R.H. Bube, A.L. Fahrenbruch, R. Sinclair, T.C. Anthony, C. Fortmann, W. Huber, C.T. Lee, T. Thorpe, Y. Yamashita, *IEEE Trans. Electron Dev.* 31 (1984) 528.
- [11] K.W. Mitchell, A.L. Fahrenbruch, R.H. Bube, *J. Appl. Phys.* 48 (1977) 4365.
- [12] T.C. Anthony, A.L. Fahrenbruch, M.G. Peters, R.H. Bube, *J. Appl. Phys.* 57 (1985) 400.
- [13] B.M. Basol, E.S. Tseng, R.L. Rod, S. Ou, O.M. Stafsudd, *Proceedings of the 16th Photovoltaic Specialists' Conference, San Diego, CA, 1982*, pp. 805–808.
- [14] B.E. McCandless, Y. Qu, R.W. Birkmire, *Proceedings of the 1994 IEEE First World Conference on Photovoltaic Conversion, Hawaii, December 1994*, pp. 107–110.
- [15] J.A. Aranovich, D. Golmajo, A.L. Fahrenbruch, R.H. Bube, *J. Appl. Phys.* 51 (1980) 4260.
- [16] P.V. Meyers, *Sol. Cells* 23 (1988) 59.
- [17] C.M. Fortman, A.L. Fahrenbruch, R. Bube, *J. Appl. Phys.* 61 (5) 1.
- [18] H.S. Ullal, *Electronic structure of electrodeposited thin film CdTe solar cells*, SERI/TP-211-3361 Report, May 1988 (Solar Energy Research Institute).
- [19] S.A. Gamboa, P.J. Sebastian, X. Mathew, H. Nguyen Cong, P. Chartier, *Sol. Energy Mater. Sol. Cells* 59 (1999) 85.

- [20] X. Mathew, P.J. Sebastian, *Sol. Energy Mater. Sol. Cells* 59 (1999) 85.
- [21] X. Mathew, P.J. Sebastian, A. Sanchez, J. Campos, *Sol. Energy Mater. Sol. Cells* 59 (1999) 99.
- [22] S.M. Sze, *Physics of Semiconductor Devices*, 2nd Edition, Wiley, New York, 1981, pp. 74–80.
- [23] R.B. Hall, V.P. Singh, *J. Appl. Phys.* 50 (10) (1979) 6406.
- [24] A.R. Riben, D.L. Feucht, *Solid State Electron.* 9 (1966) 1055.
- [25] V.P. Singh, *Proceedings of the 13th IEEE Photovoltaic Specialists Conference*, 1978, pp. 507–512.
- [26] M. Ordaz, G.B. Lush, V.J. Singh, J.C. McClure, *International Material Research Congress*, Cancun, September 1999.
- [27] J.J. Makwana, *Biasing and illumination effects in thin film CdS/CdTe photovoltaic cells*, M.S. Thesis, University of Texas at El Paso, May 1990, pp. 35–49.
- [28] S.M. Sze, *Physics of Semiconductor Devices*, 2nd Edition, Wiley, New York, 1981, p. 17.
- [29] A.L. Farenbruch, R.H. Bube, *Fundamentals of Solar Cells*, Academic Press, New York, 1983, p. 150.
- [30] S.M. Sze, *Physics of Semiconductor Devices*, 2nd Edition, Wiley, New York, 1981, p. 37, 90.
- [31] S.M. Sze, *Physics of Semiconductor Devices*, 2nd Edition, Wiley, New York, 1981, p. 87.
- [32] S.M. Sze, *Physics of Semiconductor Devices*, 2nd Edition, Wiley, New York, 1981, p. 92.
- [33] M. Eron, A. Rothwarf, *J. Appl. Phys.* 57 (6) (1985) 2275.



ELSEVIER

Solar Energy Materials & Solar Cells 70 (2001) 335–344

**Solar Energy Materials
& Solar Cells**

www.elsevier.com/locate/solmat

Light and voltage dependence of the junction transport properties of CdTe/CdS photovoltaics

D.L. Linam^a, V.P. Singh^b, J.C. McClure^{a,*}, G.B. Lush^a,
X. Mathew^c, P.J. Sebastian^c

^a *Electrical and Computer Engineering Department, University of Texas El Paso-UTEP, El Paso, TX 79968-0520, USA*

^b *Electrical Engineering Department, University of Kentucky, Lexington, KY 40506, USA*

^c *Centro de Investigación en Energía, UNAM, Temixco, Morelos, Mexico*

Abstract

The J – V curve of CdTe/CdS photovoltaics does not consist of a simple superposition of a loss current and a light generated current with a considerable loss in conversion efficiency. This paper uses capacitance/voltage measurements and J – V measurements at a variety of temperatures and light levels to develop a model for this non-superposition. It was found that a light dependent tunneling mechanism dominates at low voltages. Moreover, the tunneling takes place from a trap level within the CdTe. © 2001 Published by Elsevier Science B.V.

Keywords: Cadmium telluride; CdTe; Solar cells; Junctions; Thin films; Photovoltaics

1. Introduction

CdTe/CdS thin film cells have been extensively studied and are a leading contender for low cost mass produced solar cells. Recent references can be found in [1–3]. CdTe films have been made by a variety of techniques including CVD [4], electrodeposition [5] vacuum evaporation [6], spray pyrolysis [7], close space sublimation [8], and screen printing [9]. Interest in CdTe has continued and in the 1990's alone there were over three thousand references to work on CdTe.

The most efficient cells have been made at University of South Florida and at the National Renewal Energy Laboratory [10] with CdTe deposited by closed space

*Corresponding author. fax: +1-915-747-8036.

E-mail address: mcclure@utep.edu (J.C. McClure).

sublimation. Cells with over 10% efficiency, however, have been made by many different techniques but generally the cell efficiency suffers from a crossover in the dark and light J – V curves which indicates the junction transport properties of the cells are changed by either the presence of light or voltage or by both together. This work represents a continuation of the authors' previous work [11] in which this crossover problem, was studied using cells from three different sources (as discussed below). It was found that all cells behaved similarly when illuminated at different levels and at different temperatures. The separate effects of voltage and light level were studied, and a model for this behavior will be presented.

2. Experimental

Measurements were made on two research cells and one commercial CdTe/CdS cell. See Table 1 for details on the cells. We note that the cells have a range of efficiencies and were made by two different deposition processes. Results for all cells were similar and data will be shown for Cell B unless otherwise noted.

Capacitance versus voltage curves were made on the cells at a range of temperatures and frequencies. Space charge density was calculated by standard techniques near the junction. Temperatures were varied using a Janus cryostat and a Hewlett-Packard 4282A capacitance meter was used. Corrections for series resistance in the cell were made when calculating the capacitance.

Current Density versus Voltage curves were made for all cells between 200 and 350 K and at light levels from approximately 0.001 sun to one sun and in the dark. A solar simulator with an ENX bulb was used to illuminate the cells. Neutral density filters were used to reduce the light intensity as needed. The window of the Janus cryostat caused almost no distortion of the light spectrum. All data were collected on a personal computer for analysis. Cells exhibited both a series and parallel resistance that were removed by standard techniques [12]. Both resistances varied with light level and temperature.

3. Results and discussion

Fig. 1 shows capacitance versus voltage curves at different frequencies. We note that the capacitance increases at low frequencies indicating that a slow process such

Table 1

Cell	Efficiency (%)	V_{oc} (mV)	J_{sc} (mA/cm ²)	CdTe deposition technique
A	12.2	823	22.7	CSS ^a
B	8.9	845	16.4	CSS
C	6.6	715	20.5	SP ^b

^aCSS = Close space sublimation.

^bSP = Spray pyrolysis, commercial cell.

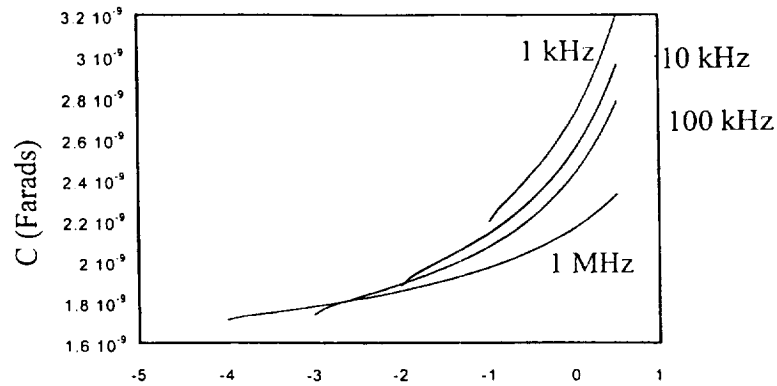


Fig. 1. Capacitance versus voltage curves at different measurement frequencies. Note larger capacitance at low frequencies where traps can be ionized.

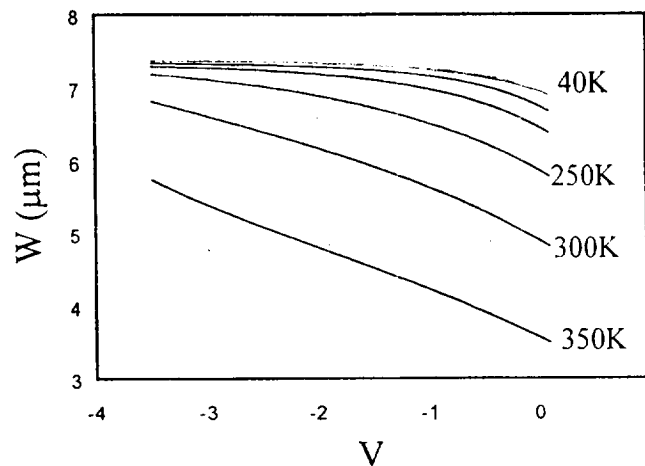


Fig. 2. Depletion region width versus voltage for various temperatures. At low temperatures traps are not ionized and lead to wider depletion regions.

as a bulk trap or interface state is active. Fig. 2 shows the depletion width curves at different temperatures. Once again, the presence of traps or interface states is indicated by the increased width at low temperatures where the traps are not thermally ionized. The traps are neutral when empty.

Fig. 3 shows the calculated charge density distribution across the depletion region at different temperatures. In the figure, W represents the distance into the CdTe and the metallurgical junction is at about $7\mu\text{m}$. A several micron wide low doping (π -type) region is seen near the junction followed by a higher doped p-region. Fig. 4 shows the presumed charge density diagram based on the above data. The T or trap layer contains the states ionized at higher temperatures.

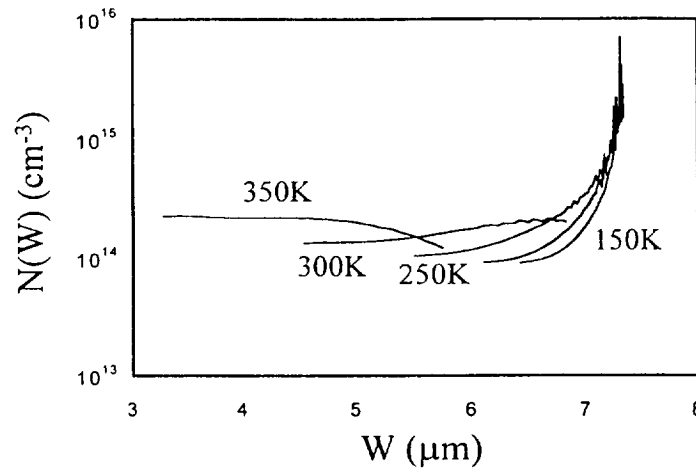


Fig. 3. Charge density at different distances into the CdTe. The metallurgical junction is at approximately $7.5\mu\text{m}$. Note wide almost intrinsic region and a highly charged region near the metallurgical junction. Temperatures are 150, 200, 250, 300, and 350 K.

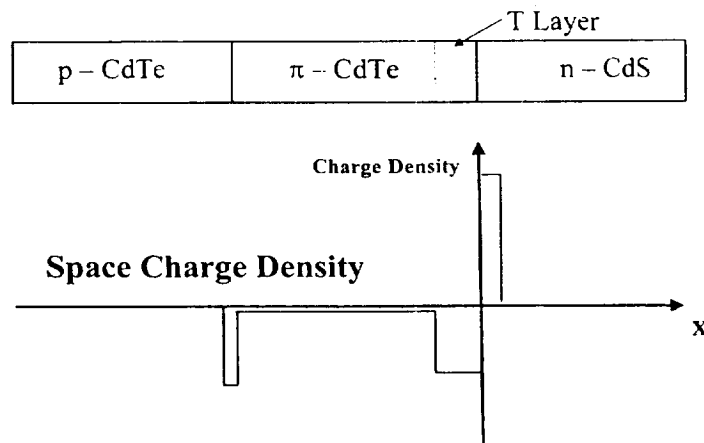


Fig. 4. Proposed charge distribution based on capacitance measurements. The occupation of the T or Trap layer is temperature sensitive.

The simplest model of solar cell performance predicts a superposition of the classic Shockley Equation [13] diode current

$$J = J_0[\exp(\alpha V) - 1] \quad (1)$$

and a voltage independent light current. In the dark, only the diode current is present and the dark and light J - V curves cannot cross. Silicon cells, for example, follow this

model quite well. The fact that the curves do cross in CdTe/CdS cells indicates that the superposition of the diode current and the light current fails, and that the junction transport mechanisms are changed by the presence of light and or voltage. This crossing of the dark and light curves reduces open circuit voltage and fill factor for a considerable loss in cell efficiency.

In Eq. (1) the reverse saturation current density, J_0 , and α ($= q/AkT$, where A is the diode ideality factor) are the diode parameters of interest. J_0 follows the equation:

$$J_0 = J_{00} \exp(-\Delta E/kT), \quad (2)$$

where ΔE is approximately $E_g/2$ and J_{00} is independent of temperature.

For current transport dominated by diffusion of carriers A should equal 1 while a dominant current mechanism of recombination/generation yields an A value between 1 and 2. Tunneling of carriers (and the presence of interface states to facilitate the tunneling) is indicated by a temperature independent value of α greater than 2.

Fig. 5 shows the J_D vs. V curves for cell B for various light levels. J_D is the diode current that is found by subtracting the light current from the measured total current. If the cell followed the Shockley Equation (1), these curves would be straight lines. We note that the slope changes with voltage. One can speak of a shallow slope at low voltage and a steeper slope at higher voltage. Furthermore, the voltage range of these slopes depends on the light level. In the dark, the high slope region starts at about 0.4 V while in full sun the high slope region starts at about 0.65 V.

Fig. 6 shows the slope (α_B) in the low voltage region (Region B) as a function of light intensity for various temperatures. We note only a very small change with temperature (particularly at higher light intensity where the data are most accurate), which indicates thermally activated transport processes cannot be important, and we

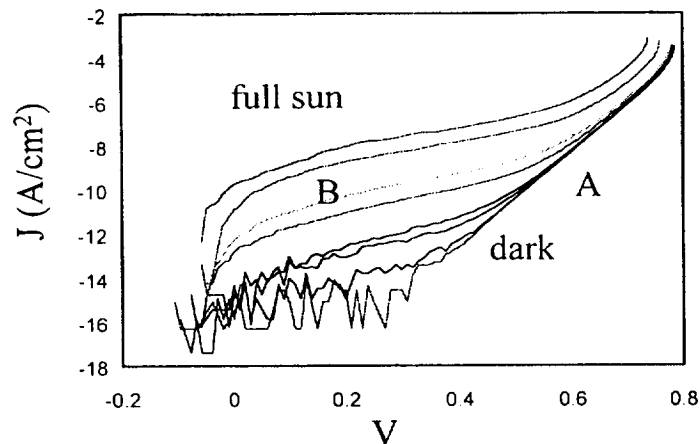


Fig. 5. Diode current for different light levels. Note presence of two distinct slopes indicating different current transport mechanism.

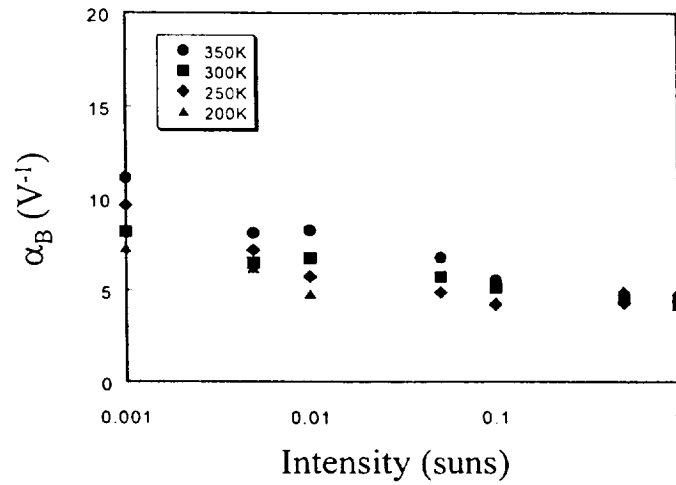


Fig. 6. Slope of curves in Fig. 1 in region B. Note very little change with temperature, but large change with illumination level.

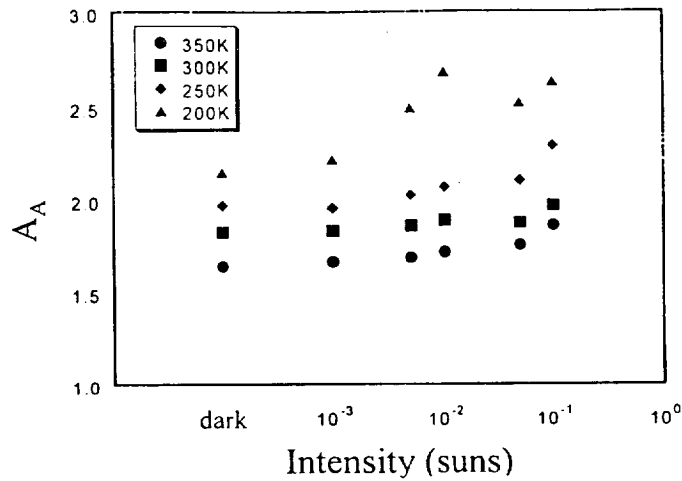


Fig. 7. Diode quality factor A_A for region A of Fig. 5. Note that the diode quality factor is independent of light intensity but changes with temperature.

can conclude that tunneling is the dominant mechanism for current transport in this region. Fig. 7 shows the diode quality factor A_A for the high slope region A for different light intensities. We note that the behavior is just the opposite to that of region B. A_A is light intensity independent but changes significantly with temperature.

Fig. 8 shows J_{OB} as determined from the Region B intercept of the curves in Fig. 5. Temperature does not affect J_{OB} appreciably, and it is linearly dependent on light

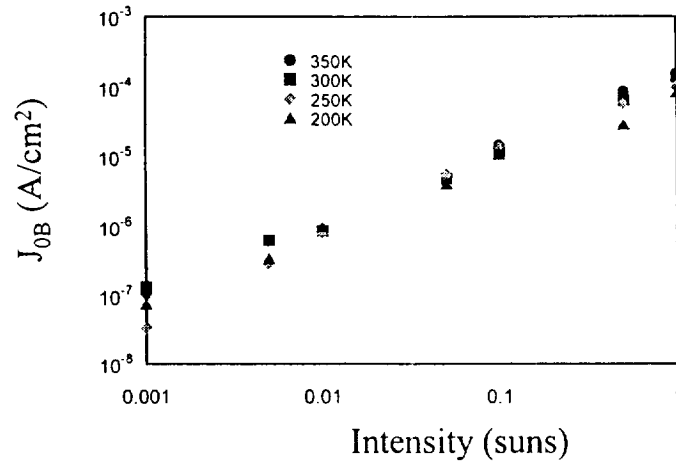


Fig. 8. Reverse Saturation Current, J_{0B} , determined from the intercept of the curves in Region B of Fig. 5. Note light sensitivity but very little dependence on temperature.

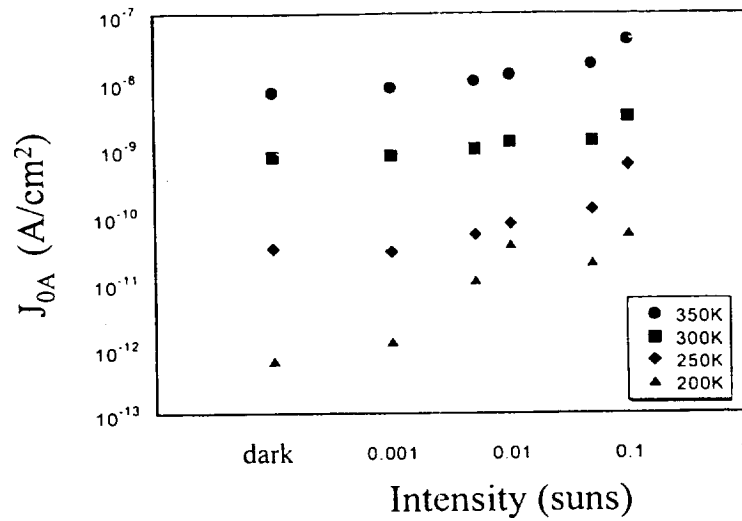


Fig. 9. Reverse Saturation Current, J_{0A} , from the intercept of the Region A curves in Fig. 5. Sensitivity to temperature but not light level is seen.

level. This again suggests that there is tunneling that is aided by high light levels in this region.

J_{0A} is shown in Fig. 9 for different light and temperature levels. Considerable variation with temperature is observed, and much smaller changes with light level are seen. Again, it can be concluded that in this region temperature activated conduction mechanisms such as diffusion and generation/recombination are active.

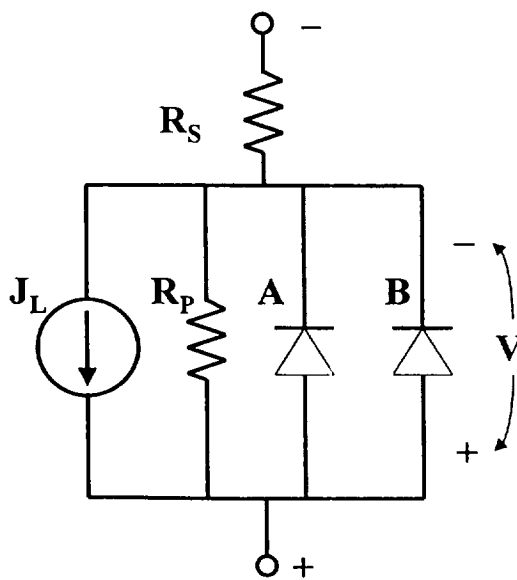


Fig. 10. Proposed equivalent circuit of the CdTe/CdS cell. The properties of diode A are temperature sensitive but light insensitivity while diode B has light sensitive but temperature insensitivity properties.

Note that the reverse saturation current in Region A, J_{oA} , is many orders of magnitude smaller than J_{oB} and the main reason for a loss in efficiency must come from the tunneling current mechanism in region B. Since light obviously facilitates this tunneling, it is believed that the tunneling takes place via an interface state whose occupancy depends on illumination.

A phenomenological model for the process can be obtained by considering the equivalent circuit shown in Fig. 10. In this figure the usual equivalent circuit of a solar cell has a second diode in parallel with the current source. One diode represents the light sensitive tunneling current and the other represents the temperature sensitive diffusion-recombination/generation current.

Data were fit to this model for a range of light intensities. Results for Cells A and B are shown in Fig. 11. It was found that J_{oA} , α_A , and α_B are the same for all light levels and that J_{oB} is a linear function of light level. This suggests that the tunneling takes place through an interface state that is progressively emptied as light level is increased.

A forward biased band diagram based on the charge distribution of Fig. 4 is shown in Fig. 12. Paths 1, 2, and 3 represent schematically current flow via diffusion, generation/recombination, and tunneling respectively. E_t represents the thermally ionizable trap level indicated by capacitance measurements. At low forward bias tunneling takes place through trap levels that are ionized by illumination and path 3 dominates. At higher bias levels the bands are bent less and paths 1 and 2 dominate regardless of light level.

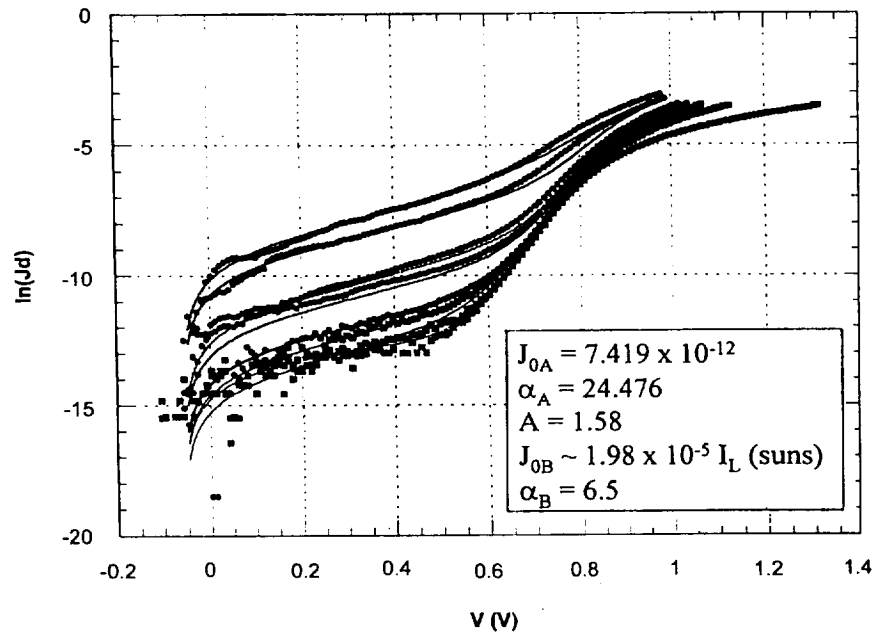


Fig. 11. Points represent experimental data and solid lines are the equations fit to the two diode model. Data is for room temperature and various light levels from 0.001 suns to 1 sun.

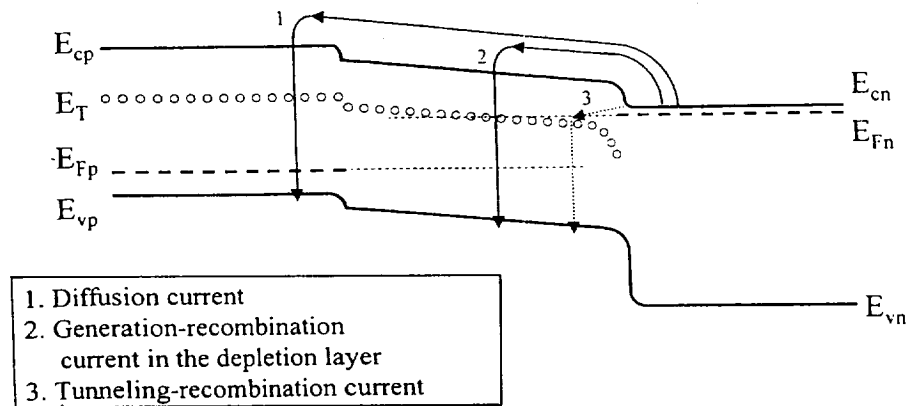


Fig. 12. Band diagram of a CdTe/CdS junction under forward bias. The three paths for loss current are indicated.

4. Conclusions

1. Carrier tunneling at the junction adversely affects the efficiency of CdTe/CdS photovoltaics.
2. The tunneling is most pronounced at high illumination levels.

3. Tunneling occurs predominantly at low voltages. At higher voltages the most important current transport mechanism is a combination of generation/recombination and diffusion with generation/recombination being the dominant mechanism.
4. The tunneling takes place through a defect state whose occupancy is changed by light level.
5. This behavior can be represented by a model of the device using two diodes in parallel with the current source.

Acknowledgements

The authors gratefully acknowledge the support of NASA BMDO Grant #21620379.

References

- [1] A.M. Herman, *Solar Energy Mater. Solar Cells* 55 (1998) 75.
- [2] T. Chu, S. Chu, *Prog. Photovoltaics: Res. Appl.* 1 (1993) 31.
- [3] D. Bonnet, *Int. J. Solar Energy* 12 (1992) 1.
- [4] D. Bonnet, H. Rabinhorst, *Proceedings of the Ninth IEEE Photovoltaics Specialists Conference*, 1972, p. 129.
- [5] S.A. Gamboa, P.J. Sebastian, M.A. Rivera, *Solar Energy Mater. Solar Cells* 52 (1998) 293.
- [6] K. Mitchell, A. Fahrenbruch, R. Bube, *J. Appl. Phys.* 48 (1977) 4365.
- [7] Y. Ma, A. Fahrenbruch, R. Bube, *Appl. Phys. Lett.* 30 (1977) 423.
- [8] Y. Tyan, E.A. Perez-Albuerna, *Proceedings of the 16th IEEE Photovoltaics Specialists Conference*, 1982.
- [9] N. Nakayama, H. Matsumoto, et al., *Jpn. J. Appl. Phys.* 15 (1976) 2281.
- [10] T.L. Chu, J.C. Chu, F.C. Britt, C.Q. Wang, H.S. Ullal, *IEEE Device Lett.* 13 (1992) 303.
- [11] V.P. Singh, D.L. Linam et al., *Solar Energy Mater.* 63 (2000) 45.
- [12] D.L. Linam, *A Model for the CdTe/CdS Junction*, M.S. Thesis, University of Texas El Paso, 2000.
- [13] A. Kaminski, J.J. Marchand, A. Laugier, *Solar Energy Mater. Solar Cells* 51 (1998) 221.